Final Report

on the research project:

Determination of Biomechanical Corridors for the Evaluation of Mechanical Hazards and Estimation of Stiffness Parameters for Future Measurement Devices

Project initiator

Institute for Occupational Safety and Health (IFA), Alte Heerstr. 111,
53757 Sankt Augustin, Germany

Project contractor

Fraunhofer IFF, Sandtorstr. 22, 39106 Magdeburg, Germany

Authors

Dr. Roland Behrens
Fraunhofer IFF
roland.behrens@iff.fraunhofer.de

Jan Zimmermann
Institute for Occupational Safety and Health (IFA)
jan.zimmermann@dguv.de

Contents

Magdeburg, November 3, 2021

1 Introduction

Fraunhofer IFF conducted several human subject studies from 2015 to 2019 on behalf of the Institution for the Woodworking and Metalworking Industries (BGHM) and with research funding from the German Social Accident Insurance (DGUV). In these studies, we examined the responses of over 100 individuals with impact and pinching loads applied by a pendulum and an algometer. Fraunhofer IFF used the data from the studies to calculate pressure and force limits for quasi-static and transient human-robot contacts and all 29 body parts listed in ISO/TS 15066. The limits enable cobot users to assess the hazard potential of their robots operating near humans without safety fencing. Moreover, the new limits constitute promising successors to the preliminary limits listed in ISO/TS 15066 since the existing limits are based on a literature survey and have never been verified by experiments with human subjects.

Along with biomechanical limits, ISO/TS 15066 also specifies a set of stiffness parameters with which instruments for measuring cobots' hazard potential must comply. The parameters ensure that the instruments correctly replicate the human body's biomechanical response to impacts or pinching. Since the stiffness parameters were taken from the same literature survey as the current ISO/TS 15066 limits, they have never been verified experimentally. Replacing the preliminary limits only makes sense biomechanically when the stiffness parameters are replaced as well. Otherwise, tests of cobots using the new limits with the old stiffness parameters would certainly deliver incorrect results. This could ultimately pose a serious health risk to humans working with cobots.

Fraunhofer IFF conducted a follow-up study in collaboration with the BGHM and the Institute for Occupational Safety and Health (IFA) with the intention of specifying new stiffness parameters based on the same data used to specify the new limits. The study included the following work packages:

- development of biomechanical corridors describing the natural biomechanical response of the body locations listed in ISO/TS 15066,
- integration of a statistical model that relates corridors' curves to specific percentiles,
- development of a piecewise linear approximation of corridors' reference curves to derive stiffness parameters for future measuring instruments, and
- clustering of the stiffness parameters to reduce their number.

2 Methods and Materials

Biomechanical corridors, i.e., force-deformation curves indicating human response to impact load, serve as the basis for the new stiffness parameters. First, Fraunhofer IFF developed a method for creating such corridors from human subject study data. The method comprises a statistical model that enables us to relate the corridors' curves to specific force and deformation percentiles. Additionally, an approximation method was developed to estimate the desired stiffness parameters from the corridor curves that describe the response of a target population' percentile. Finally, IFA and Fraunhofer IFF analyzed the stiffness parameters obtained from the corridors for similarities. All similar sets of parameters were subsequently clustered. All the data processed in this study come from the human subject studies (see section 1).

2.1 State-of-the-Art

Biomechanical corridors map contact force over tissue deformation to describe the deformation of a human body part under load. An individual corridor is always related to specific load conditions, which include the shape of the object exerting force or the rate of deformation. Such corridors commonly serve as a reference for anthropomorphic test devices (ATD) to ensure they have a humanlike response when subjected to impact. As the example in Figure 1 shows, a biomechanical corridor typically has a lower and an upper boundary curve indicating the variances of the data from which the corridor was created. Corridors can also have another curve within the boundaries, which usually correlates with the averaged force or deflection data, to illustrate the characteristic response. Adding or subtracting their standard deviations to or from the characteristic curve yields the lower and upper boundaries (Shaw et al. 2006).

Several methods for developing biomechanical corridors exist. Most methods can be divided into three separate steps, each step utilizing a specific technique to process the study data. Essential to all the methods is processing the data in such a way that the shape of the individual response curves is retained (Kim et al. 2013) and discontinuities in the corridor curves are prevented. The first step deals with the variability of individuals' body parameters and is especially relevant when comparing experimental results from human subject tests with an ATD's response or vice versa (Morgan et al. 1986). The scaling technique devised by Eppinger et al. (1984) is used for this purpose most frequently. It reduces the variability between individual subjects by factors that convert the experimental data from different subjects with individual geometric and inertial properties into a standard anthropometry.

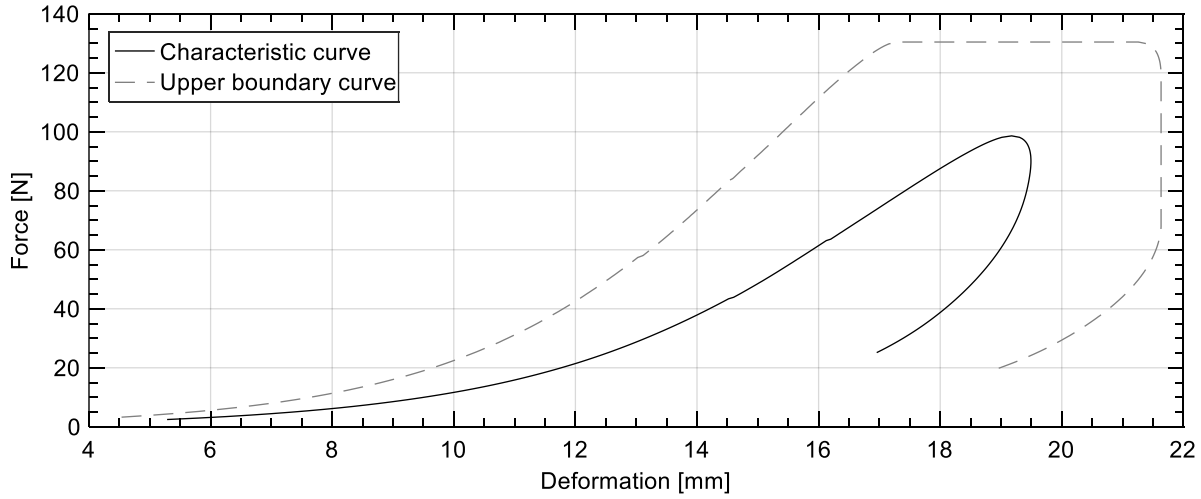

Figure 1. Biomechanical corridor with typical hysteresis

The second processing step aligns the force and deformation signals recorded in the human subject tests with each other. Several criteria exist for signal alignment. Other studies predominantly use the zero-force criterion. It modifies the signals' time axes so that the time of initial contact coincides with time zero in all signals (Lessley et al. 2002). The peak value criterion shifts the signal's time increments so that all peaks in the signal coincide with time zero. A modified variant of the peak value criterion employs the first appearance of a specific percentage of the peak values

for alignment. The third criterion is cross-correlation (Maltese et al. 2002; Nusholtz et al. 2009). It optimizes all signals simultaneously until they are in-phase and the cumulative variance between all pairs is minimal (global least-square differences). Maltese et al. (2002) modified the criterion. Instead of comparing the signals pairwise, this technique aligns the signals to a baseline signal that is the best representation of all. Nusholtz et al. (2009) improved the alignment technique so that it first searches for a pair of signals with the highest cross-correlation coefficient. By eliminating the need to select a baseline, it compensates the user's influence on the final corridor's shape (Hsu und Nusholtz 2005). Once the pair with the best cross-correlation has been identified, the technique aligns the time axes of the paired signals and averages them to synthesize a new signal. Then, the new signal replaces the paired signals in the set of all signals. The procedure is repeated until the set includes just one final signal. Next, all signals are aligned to the last signal so that the sum of the cross-correlation coefficients is the maximum. Afterward, the entire procedure, from identifying pairs to aligning the signals to the final signal, is repeated until the sum of the correlation coefficient converges. Other criteria for signal alignment, e.g. those devised by Sun et al. (2016), are not widely used in biomechanical research and thus not discussed here.

The third step finally creates the corridor curves. Cavanaugh et al. (1986) and Morgan et al. (1986) present a time-based technique for this purpose. Once they have aligned the force-time signals using the force-zero criterion, they calculate the average and standard deviation of the force values at each time step in the signals to create the corridor's curves. The technique also has to be applied to the deformation-time signals to obtain two separate time-based corridors for force and deformation. Cross-plotting both time-based corridors ultimately removes the time dimension and delivers the response corridor. Maltese et al. (2002) demonstrated that the time-based technique devised by Cavanaugh et al. (1986) can be combined with a correlation criterion to obtain more accurate corridors.

Lessley et al. (2002) and Shaw et al. (2006) criticize the failure of the time-based technique to retain the characteristic shape of the natural human response and therefore propose a deformation-based technique. In the first step, their technique normalizes the deformation-time signals by dividing all sampled deformation values by the maximum deformation so that the magnitude of all signals ranges from 0 to 1. An interpolation routine ensures that the normalized signals only consist of equidistant normalized deformation values, i.e., the distance from one normalized deformation value to both neighbors is always equal and constant. Then, the technique averages the values of the force-time signals that coincide with the times at which the normalized deformation signals reach a given normalized deformation value. Repeating the averaging for a list of ascending normalized deformation values between 0 and 1 yields a list of force values. Then, the averaged force values are plotted as a function of the normalized deflection multiplied by the mean of all maximum deformation values derived from the non-normalized signals. The plot ultimately delivers the corridor's characteristic curve. The upper and lower boundaries were derived from the pointwise standard deviation of the force and deformation values. Unlike the time-based technique, this technique does not require signal alignment (i.e. the second processing step; see above). Other development methods with less relevance for our study can be found in articles by Bolte et al. (2003), Stemper et al. (2004) and Raymond et al. (2009).

The points defining the characteristic curve typically correspond to the mean value of the data. The points defining the lower and upper boundaries, however, are not defined precisely. They can be extracted from either a rectangular or an ellipsoidal region around the points of the characteristic curves. Both regions' dimensions are defined by the standard deviations of force and tissue deformation. A rectangular region is always centered on the points of the characteristic curve. The negative and positive standard deviation values correspond to the length of the rectangle's edges. The ellipse approach uses the standard deviation values as the two radii of an ellipse enclosing the related point of the characteristic curve. Each of the rectangle's or the ellipse's two outermost points correspond to one point on the corridor's upper and lower boundaries.

2.2 Modified Development Technique

This study's corridors are intended to describe the biomechanical response of working-age individuals since they are most likely to work with cobots. The data come from tests with individuals from this target population and were processed into corridors without scaling them to any specific anthropomorphic baseline.

2.2.1 Force Normalization

Since the literature survey (see section 2.1) revealed that only the deformation-based technique first presented by Lessley et al. (2002) retains the shape of the individual biomechanical responses, we decided to use their technique. Even though the same data were processed, this produced corridors with maximum force values that do not match the force limits. The deformation-based technique had to be modified to ensure a perfect match. Instead of the deformation signals, our modified technique normalizes the force signals $F_i(t)$ by dividing their discreetly sampled values $F_i(t_k)$ pointwise by the maximum values $\hat{F}_i = F_i(\hat{t}_i) = \max F_i(t)$

$$F_i^*(t_k) = \frac{F_i(t_k)}{\hat{F}_i}$$

where $F_i^*(t_k) \in [0; 1]$. From this point on, the development process is identical to the deformation technique. An interpolation routine resampled $t_k \rightarrow t_\kappa$ the $F_i^*(t_k)$ so that all values in $F_i^*(t_\kappa)$ had a constant distance of ΔF^* to their neighbors

$$F_i^*(t_\kappa) - F_i^*(t_{\kappa-1}) = \Delta F^* \quad .$$

A second interpolation routine plotted the original deformation signals $d_i(t)$ and force signals $F_i(t)$ to the new time increments t_κ

$$d_i(t_k) \rightarrow d_i(t_\kappa) \quad \text{and} \quad F_i(t_k) \rightarrow F_i(t_\kappa) \quad .$$

We obtain a set of N time increments $t_{p,i}$ with $i \in \{1; 2; \dots N\}$ from $F_i^*(t_\kappa)$ for a given percentage value $p \in \{0, \Delta F^*, 2\Delta F^* \dots 1\}$

$$F_i^*\left(t_{p,i}\right) = p \quad .$$

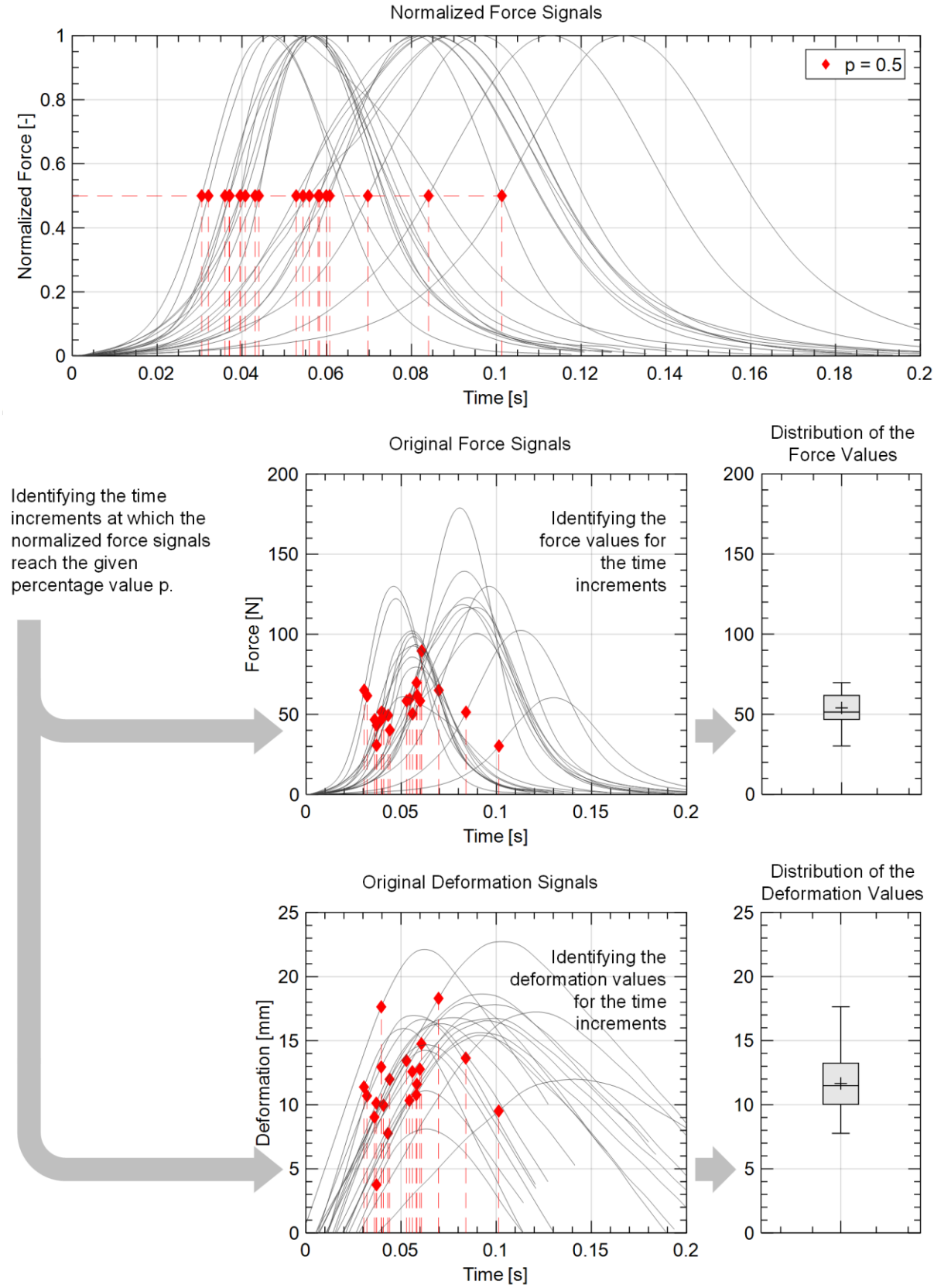

Figure 2. Sampling technique for calculating specific data points of the corridor curve

The time increments $t_{p,i}$ can then be used to extract a set of deformation values $d_{p,i}$ and force values $F_{p,i}$ from $d_i(t)$ and $F_i(t)$, respectively. All values $d_{p,i}$ and $F_{p,i}$ belong to the compression phase (i.e. the phase from initial contact to maximum force) when their corresponding time increments $t_{p,i}$ satisfy $t_{p,i} \leq \hat{t}_i$. All others belong to the restitution phase (i.e. the phase from maximum force to end of contact) and correspond to time increments$t_{p,i}$ that satisfy $t_{p,i} > \hat{t}_i$. Whenever a force signal's curve includes local minima, multiple time increments $t_{p,i}$ can result in multiple deflection values for the same p value. The mean of these deflection values was used as a corridor point to resolve this ambiguity.

2.2.2 Statistical Model

Any p value yields N individual deformation and force values, both for the compression and restitution phase. Unlike other techniques, the values of a specific p were treated as a sample containing randomly distributed observations. In the human subject studies, we demonstrated that the data are log-normally distributed with the mean μ_X and the standard deviation σ_X

$$\ln X \sim \mathcal{N}(\mu_X, \sigma_X^2) \quad .$$

We assume the same for the data arranged in samples. An Anderson-Darling test confirmed our assumption for the majority of samples. We used the maximum likelihood estimation to estimate μ_X and σ_X from the samples for both force $X \leftrightarrow F_{p,i}$ and deflection $X \leftrightarrow d_{p,i}$

$$[\tilde{\mu}_X, \tilde{\sigma}_X] = \arg\max_{\mu_X, \sigma_X} \prod_{i=1}^{N} f(x_i; \mu_X, \sigma_X)$$

with the normal distribution function

$$f(x_i;\ \mu_X, \sigma_X) = \frac{1}{\sigma_X} \varphi\left(\frac{\ln x_i - \mu_X}{\sigma_X}\right) \quad .$$

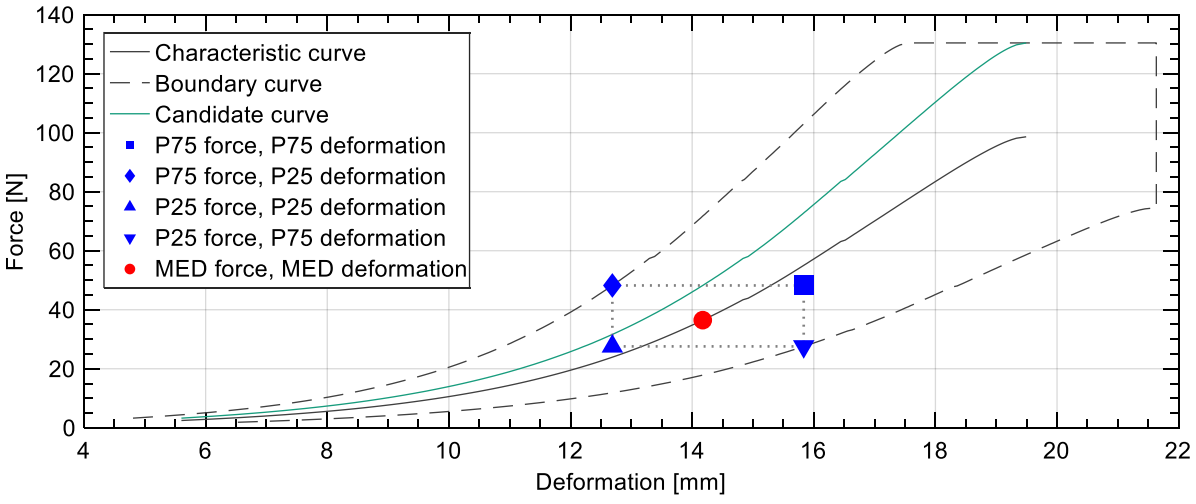

Figure 3. Development of the corridor's boundary curves

The estimates $\tilde{\mu}_X$ and $\tilde{\sigma}_X$ can then be used to calculate the corresponding quantile values for the 25th, 50th and 75th percentile from inverse cumulative distribution function

$$\mathcal{F}(x_i;\, \mu_X, \sigma_X) = \Phi\left(\frac{\ln x_i - \mu_X}{\sigma_X}\right) \quad .$$

Since we used the same distribution model as we did in the human subject studies, the corridors' maximum force values equal the force-based limit values. This coincidence could only be obtained by normalizing the force signal instead of the deformation signals, as Lessley et al. (2002) propose.

2.2.3 Corridor Development

The percentile values calculated with the statistical model can then be used to plot the corridor in the force-deformation plane. As in other development techniques, the corridor's characteristic curve is obtained from the 50th percentile points. A rectangle can be drawn at each point on characteristic curve. The distance between the rectangle's sides and the point on the characteristic curve correspond to the 25th and 75th percentile of the same force and deformation data from which the point on the characteristic curve was calculated. The outermost points of all rectangles that can be drawn along the characteristic curve yield the corridor's lower and upper boundary curves. At the start of the compression phase, for instance, the force values for the 75th percentile and the deformation values for the 25th percentile are equivalent to points on the upper boundaries until the characteristic curve reaches its maximum. Conversely, the points on the lower boundary are usually derived from the force values for the 25th percentile and from the deformation values for the 75th percentile. Figure 3 presents the development of the corridor curves.

The curve describing the median of the deformation values and the 75th percentile of the force values is an appropriate candidate curve that instruments for collision measurement ought to reproduce to perform like the human body when struck by a robot.

2.2.4 Piecewise-Linear Approximation

The general shape of the candidate has to be analyzed in order to obtain stiffness parameters from it. As Figure 3 shows, the curves of the compression phase typically consist of a nonlinear toe followed by an approximately linear branch. The force over deformation in the range of the toe rises progressively until a transition point is reached. Beyond this point, the relation between deformation and force becomes and remains proportional up until the force reaches its maximum value (see Figure 4). Using two piecewise-linear curves to approximate both parts yields a sufficiently accurate representation of the whole candidate

$$F_C(d_j) \approx F_C^*(d_j; c_1, c_2, d_T, F_T) = \begin{cases} c_1(d_j - d_T) + F_T & d_0 \le d_j < d_T \\ c_2(d_j - d_T) + F_T & d_T \le d_j \end{cases}$$

where d_0 indicates the initial deformation of the curve's toe and (d_T, F_T) the transition point at which the curve becomes linear. The parameters c_1 and c_2 are the slope parameters of the approximation lines. Their slope parameters and the point of their intersection (transition point) should produce a minimum square error when they are compared with the candidate curve. Assuming the linear part of the curve ends at d_e, the following expression yields an optimal solution for range $d_0 \le d_j \le d_e$

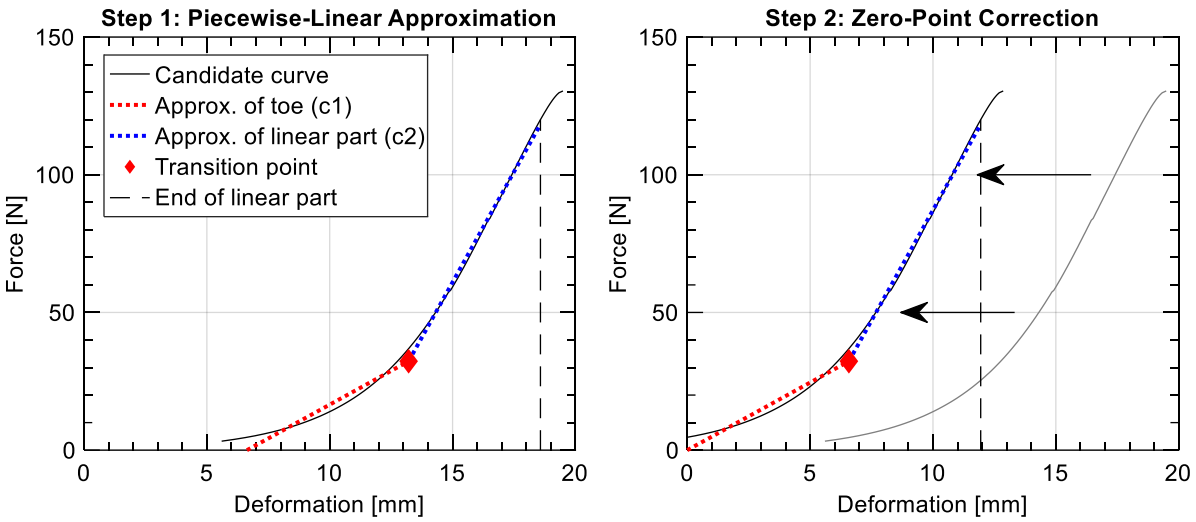

Figure 4. Piecewise-linear approximation of the response curve by two lines (left); zero-point correction by shifting all curves so that the approximation of the curve's toe intersects with the origin of the force-deformation plane

$$\boldsymbol{\eta} = \arg\min_{\boldsymbol{\eta}} \sum_{j=1}^{N} \{F_C(d_j) - F_C^*(d_j;\boldsymbol{\eta})\}^2$$

where $\boldsymbol{\eta}$ represents the slope parameters and the transition point

$$\boldsymbol{\eta} = [c_1 \;\; c_2 \;\; d_T \;\; F_T] \quad .$$

As mentioned, d_e indicates a second transition point at which the curve becomes nonlinear again. Unlike d_T, the value of d_e cannot be determined automatically, e.g., by optimization, since the corridors' shapes vary considerably among all body parts tested. The decision was made, therefore, to select d_e manually as a boundary condition for finding $\boldsymbol{\eta}$.

Once the parameters had been determined, the zero-point of the curve was shifted so that the linear approximation of the toe starts at $d = 0$. The displacement Δd is specified by

$$\Delta d = d_T - \frac{F_T}{c_1} \quad .$$

The adjustment is linear and does not affect the approximation slopes (see Figure 4, right). It solely serves to shorten the initial contact phase described by the curve's flat toe. Removing this part of the curve is technically irrelevant to robots since their collision sensors and safety functions are unable to detect the low forces that occur during this contact phase.

2.3 Clustering

Body locations with similar slope parameters should be clustered into groups to reduce the number of parameters that later dictate the design specifications of measuring instruments. Technically, the toe of the candidate curve correlates to a small amount of energy involved in robot collision. For this reason, the parameter c_1 has little effect on the overall contact event or the maximum contact force. The primary objective of clustering was thus to identify a minimum num-

ber of classes to which the different values of parameter c_2 can be assigned. Each class is associated with a spring rate. Whenever the relative error between the associated c_2 value and one of the class-defining spring rates was minimal, we assigned the individual body location associated with c_2 to the cluster associated with the best fitting spring rate. Moreover, the relative error should never exceed 25% in order to avoid optimistic assignments (i.e. the assigned body location is actually 25% stiffer than the class-defining spring rate that ought to replicate the body location).. Section 3.3 presents the class values to which we assigned the c_2 values derived from the candidate curves.

2.4 Available Data

Table 1 presents the work plan of the studies conducted by Fraunhofer IFF. The data from experiments with over 100 human subjects include contact force and tissue deformation, both of which were measured over time. Several constraints explained below precluded the use of all data to create corridors. One constraint in particular had potential to affect the validity of the corridors and therefore had to be compensated by scaling the corridors' curves following their creation.

2.4.1 Limitations

We were only able to use the data from impact tests with the F-Q10 contact body (see Figure 5) to develop corridors. We could not use the data from tests with F-C30 because it was made of compliant foam . We were unable to compensate the deformations measured with F-C30 since they include the deformation of the contact body itself.

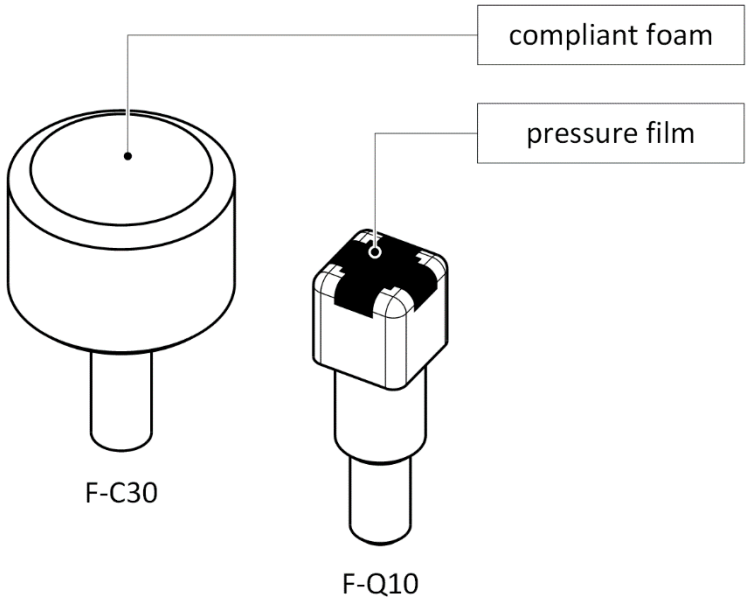

Figure 5. Contact bodies employed (F-C30 made of compliant foam has a circular area of 30 mm in diameter; F-Q10 made of aluminum has a rectangular area of 14 x 14 mm. All edges and corners were rounded to a radius of 2 mm.)

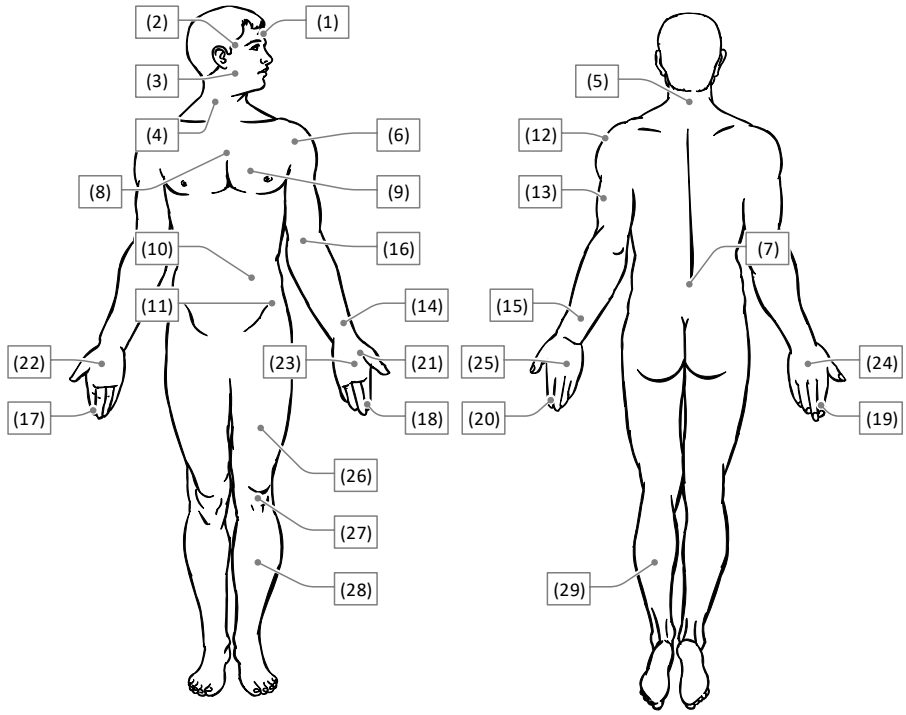

Head and neck
(1) Forehead
(2) Temple
(3) Masticatory muscle
(4) Neck muscle
(5) 7th Cervical vertebra

Trunk
(6) Shoulder joint
(7) 5th lumbar vertebra
(8) Sternum
(9) Pectoral muscle
(10) Abdominal muscle
(11) Pelvic bone

Upper extremity
(12) Deltoid muscle
(13) Humerus
(14) Radial bone
(15) Forearm muscle
(16) Arm nerve

Lower extremity
(26) Thigh muscle
(27) Kneecap
(28) Middle of shin
(29) Calf muscle

Hand and fingers
(17) Forefinger pad D
(18) Forefinger pad ND
(19) Forefinger end joint D
(20) Forefinger end joint ND
(21) Thenar eminence
(22) Palm D
(23) Palm ND
(24) Back of the hand D
(25) Back of the hand ND

Figure 6. Body locations in need of limits to refine FBHM 080 and ISO/TS 15066

The data from the pinching tests done with F-Q10 were not incorporated, either. The low indentation velocities applied in those tests produced flatter corridors and lower slope parameters. This might be because the viscosity of soft tissue establishes a relationship between the slope of contact force (as a function of time) and indentation speed (deformation rate). The force signals from the pendulum tests have significantly higher slopes because the biomechanical response of soft tissue is rate dependent. They provide, therefore, the sole basis for creating the corridor curves from which we can derive conservative stiffness parameters that never lead to optimistic results (e.g., lower contact forces) when assessing a cobot. Since the data indicated that impact mass does not affect corridors' shape, it was possible to merge the data from tests with different masses.

2.4.2 Scaling

Tests with F-Q10 were solely conducted to determine pressure limits. To this end, the size and shape of F-Q10 were specifically designed to replicate semi-sharp contacts in which the peak pressure within the contact area is more relevant than the force for determining whether the contact caused a specific form of biomechanical stress (e.g., pain). Force limits were calculated from data acquired with F-C30, though. Since the contact area is significantly larger than that of F-Q10, it is suitable for replicating blunt contact. The maximum forces reached in the tests with F-Q10 are significant lower than those reached in the tests with F-C30 because of the contact bodies' different sizes.

As mentioned in the previous section, signals from tests with F-C30 cannot be used to develop the desired corridors. The development has to be done with F-Q10 data and delivers corridors with maximum forces that are inevitably below the force limits. This makes it necessary to transform the candidate curves so that their maximum force values precisely correspond to the associated force limits in order to ensure that the corridors nevertheless describe human responses under forces in the region of the force limits.

In 2019, Fraunhofer IFF conducted a human subject study contracted by Panasonic to examine the effects of a contact body's size on humans' pressure-pain threshold (Pungrasmi et al. 2019). Impact and pinching loads were applied to the subjects by different contact bodies (F-Q5, F-Q10, and F-Q20) shaped like F-Q10 but with different dimensions. The analysis of the data revealed that the averaged maximum deformations were similar for all contact bodies, while the averaged maximum forces differed significantly. It turned out that the magnitude of the contact force depends on the size of the contact body. Based on these findings, we can presume that the extent of deformation determines whether the loading of a body part causes pain. In other words, the size of the object in contact with the human body appears to have an effect on the maximum acceptable contact force but not on deformation.

Given these findings, the candidate curves developed from F-Q10 data must be transformed into curves describing the response for a rigid contact body shaped like F-C30 by multiplying them with

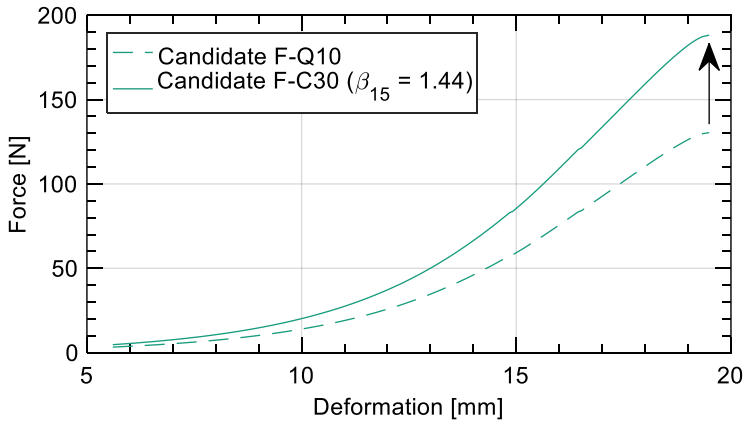

Figure 7. Transformation of the candidate curves by scaling them up to the force limit (here, from 118 N to 170 N)

Table 1. The work plan of all studies conducted from 2015 to 2019 (ond. = only body locations on the non-dominant hand)

Study no.	1		2	3		
Subject group no.	#1	#2	#3	#4	#4	#5
Subject group size	40	20	20	20	20	10
Body locations (see Figure 6)	(6) ⋮ (29)	(6) (7) (11) ⋮ (29)	(6) (7) (11) ⋮ (29) ond.	(1) ⋮ (3) (5)	(1) ⋮ (3) (5) (8) ⋮ (10)	(1) ⋮ (3) (5) ⋮ (29)
Load type						
Quasi-static (pinching)	✓			✓		✓
Transient (impact)		✓	✓		✓	
Contact body (see Figure 5)						
F-Q10 (pressure limits)		✓*	✓*		✓*	✓
F-Z30 (force limits)	✓	✓	✓	✓	✓	
Impact mass (only for impact tests)						
~6.5 kg		✓	✓		✓	
~16.5 kg		✓	✓		✓	
Repeats	5	1	1	3	1	3
Values measured						
Contact force	✓	✓	✓	✓	✓	✓
Tissue deformation	✓	✓	✓	✓	✓	✓
Contact pressure		(✓)	(✓)		(✓)	✓

$$\beta_i = \frac{\hat{F}_i}{\hat{F}_i^{FQ10}}$$

where $\hat{F}_i$ denotes the force limit for transient contacts (impacts) from the human subject studies, $\hat{F}_i^{FQ10}$ the force limit for transient contacts from the F-Q10 data, and i the identification number of the body location specified by ISO/TS 15066. The candidate curves were transformed first and then approximated using the method presented in section 2.2.4. Figure 7 presents the results of the transformation of the candidate curves for body location (15).

3 Results

We developed biomechanical corridors for altogether 24 body locations from the data collected in the human subject studies (data from dominant D and non-dominant ND body locations were combined.) Then, we derived stiffness parameters from all corridors' candidate curves. A MATLAB program automatically processed the data. The program implemented the force normalization and data resampling procedures as well as the statistical model that we have developed to calculate used to calculate specific percentile values from resampled force and deformation values. It additionally approximated the nonlinear candidate curves with two lines and clustered the second line's slope parameters with specified spring rates. The following provides a brief overview of our results.

3.1 Biomechanical Corridors

Only the compression phase of the biomechanical response was of interest in this study since the restitution phase is irrelevant to the design of a pressure-force measurement device (PFMD). The points on the characteristic curves of the corridors developed with the statistical model correspond to the median of the resampled force and deformation signals. The data points on their boundary curves correspond to the outermost points of the rectangles enclosing the points on the characteristic curves, the rectangles' side lengths corresponding to the permutation of the 25th and 75th percentile of the resampled force and deformation signals. The corridors' candidate curves correspond to the 75th percentile of the force and the 50th percentile (median) of the deformation. They describe the desired response future PFMDs must replicate. We selected the 75th percentile for force so that the maximum force of the candidate curves matches the force limits from the human subject studies (see section 1).

Figure 8 shows the corridor we developed for body part (15), forearm muscle. The graphs of all corridors can be found in Appendix A. Closer examination of the graphs reveals that the linear section at the end of the compression phase is less clear for some corridors or does not reach the maximum force values, as is the case for body location (12) or (28), for instance. Most likely, this is attributable to the inability to secure the body parts fully during the experiments and indicates that impact forces caused the body part under test to move slightly. The deformation signals from such tests consequently include body part displacement in addition to tissue deformation. Displacement could not be compensated since the testing system had just one position sensor. We observed in the tests, however, that hard-to-secure body parts did not begin moving until after the contact force had passed the linear section of the response.

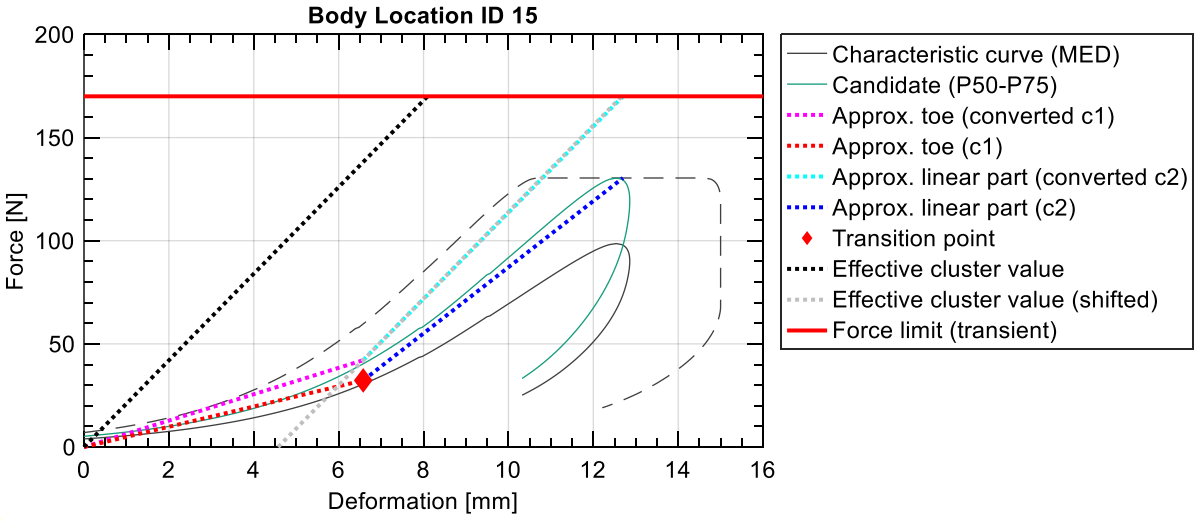

Figure 8. Compression phase of the biomechanical corridor from testing at body location 15 (forearm muscle), including the piecewise-linear approximation of the candidate curve

3.2 Stiffness Parameters

The slope parameters obtained by the optimal and piecewise-linear approximation of the candidate curves delivered the desired stiffness parameters for the force-pressure measurement device. Along with the stiffness parameters, the approximation ascertained transition points at which the approximation lines defined by the slope parameters intersect. The candidate curve correlates with the 50th percentile of the deformations and the 75th percentile of forces measured in the human subject tests. The biomechanical limits are based on the same percentiles. The maximum contact forces of most candidate curves differ slightly from the force thresholds, though, since those with heavily skewed curves were treated as outliers that had to be eliminated in order to avoid discontinuities in the candidate curves. Table 2 presents the slope parameters and the transition point from the piecewise-linear approximation of the candidate curves. The deformation of the transition point had been shifted so that the first line defined by c_1 intersects the origin of the force-deformation plane (see Figure 4).

Table 2. Slope parameters and transition point obtained from the approximation of the corridors' candidate curves (developed from the 50th percentile of the deformation values and 75th percentile of the force values measured in the human subject tests)

Body part	Body location	c_1 [N/mm]	c_2 [N/mm]	d_T [mm]	F_T [N]	$\hat{F}$ [N]
Head and neck	(1) Forehead	90.1	232.6	0.3	29.0	130
	(2) Temple	10.6	35.6	1.3	13.2	80
	(3) Masticatory muscle	4.3	16.0	3.2	13.8	70
	(4) Neck muscle*	5.2	22.9	3.2	16.6	80
	(5) 7th cervical vertebra	5.7	19.2	2.9	16.6	80
Trunk	(6) Shoulder joint	5.1	18.4	3.3	16.8	110
	(7) 5th lumbar vertebra	11.6	37.8	4.9	56.7	200
	(8) Sternum	10.9	25.6	1.3	13.8	110
	(9) Pectoral muscle	3.5	9.0	6.1	21.0	120
	(10) Abdominal muscle	1.1	1.7	20.2	22.1	80
	(11) Pelvic bone	18.5	78.2	1.8	33.4	150
Upper extremities	(12) Deltoid muscle	2.9	10.8	8.7	25.3	130
	(13) Humerus	7.6	23.7	3.9	29.6	160
	(14) Radial bone	15.2	27.2	3.1	47.0	190
	(15) Forearm muscle	6.4	20.9	6.6	42.1	170
	(16) Arm nerve	5.2	18.0	8.6	45.2	150
Hand and fingers	(17)/(18) Forefinger pad	23.4	66.5	3.4	78.1	410
	(19)/(20) Forefinger end joint	39.1	89.2	2.2	87.6	400
	(21) Thenar eminence	10.7	29.5	7.3	78.4	260
	(22)/(23) Palm	15.5	52.0	6.4	99.2	360
	(24)/(25) Back of the hand	28.2	48.0	2.5	69.5	250
Lower extremities	(26) Thigh muscle	4.4	12.3	17.1	74.9	220
	(27) Kneecap	36.1	72.4	1.2	44.0	310
	(28) Middle of shin	38.7	143.5	1.2	46.1	270
	(29) Calf muscle	5.5	14.6	17.8	98.2	280

*) Estimated (see section 4.1); c_1 is the slope parameter of the line representing the toe of the corridor curve; c_2 is the slope parameter of the line representing the linear section of the corridor curve; d_T and F_T specify the transition point between both lines; $\hat{F}$ is the force limit for transient contacts.

3.3 Stiffness Parameter Clustering

Accurately reproducing the approximated candidate curves would have required combining a mechanical spring with a soft layer of foam or another highly compliant material. Compliance is restricted, however, whenever pressure has to be measured. Films typically used to measure pressure must be affixed to the top side of the soft layer to take optimal measurements. Films must be prevented from deforming severely to prevent wrinkling the sensor material, thus ensuring accurate measurements. This constraint translates directly into a constraint on the soft layer's compliance. Dispensing with a soft layer at all is not recommended since the film would then have to be affixed to the PFMD's metal impactor, which would result in unusable measurements. We performed collision experiments with different materials and took pressure measurements to identify a minimum compliance of the soft layer. The tests revealed that materials with a shore type A hardness of 70 (SH70) and a thickness of 7 mm keep the pressure films from wrinkling.

The commercially available $N = 5$ springs listed in Table 3 define the possible clusters. The optimization algorithm mentioned in section 2.3 is used to identify a subset with $n \leq N$ of these springs with rates C that best represent the c_2 values from the candidate curves best. The optimization must take into account that a PFMD's overall stiffness C^* (effective rate) differs from the rate of the installed spring when a soft layer is added to the PFMD's impact plate. We conducted indentation tets to ascertain C^* that includes the contribution of both springs listed in Table 3 and a SH70 layer. The PFMD under test was subjected to a pinching load applied by F-Q10. The force was increased to 500 N at a constant deformation rate of 1 mm/s. Since the forces and deformations recorded indicated that the PFMD under load responds almost linearly, a single value for C^* can express the effective rate of each combination. The C^* values measured are significantly lower than the spring rates, as shown in Table 3. A separate measurement with a SH70 layer alone obtained a material stiffness of 130 N/mm.

All C^* values are only valid for pinching loads transferred by a contact body shaped like F-Q10. We decided to use only one SH70 layer to be able to take pressure measurements. Although the use of soft layers with lower shore values would have replicated the natural biomechanical responses more accurately, the need to evaluate pressure during robot contacts had higher priority.

Assuming that the dimensions of typical collision points on a robot system are usually larger than the dimensions of F-Q10, the effective cluster values C^* must be used instead of C in optimization. Moreover, before the algorithm could determine a minimum number n of reasonable clusters, it had to identify a tuple of C^* values that result in a minimum cumulative squared error

$$\left(\check{C}^*_{i_1}, \ldots, \check{C}^*_{i_n}\right) = \arg\min \sum_{b=1}^{N_B} e_b^2\left(C^*_{i_1}, \ldots, C^*_{i_n}\right)$$

Table 3. Rate parameter C of commercially available springs and their effective spring rate C_i^* when combined with a SH70 (shore type A hardness of 70) soft layer and a thickness of 7 mm

i	C_i [N/mm]	C_i^* [N/mm]
1	10	9.3
2	25	21.0
3	40	30.6
4	75	47.5
5	150	73.9

where N_B is the number of different body locations and e_b the minimum individual relative error

$$e_b\left(C_{i_1}^*, \dots, C_{i_n}^*\right) = \min\left\{\varepsilon\left(C_{i_1}^*, c_2^b\right), \dots, \varepsilon\left(C_{i_n}^*, c_2^b\right)\right\}$$

with

$$\varepsilon(\gamma_0, \gamma_1) = \frac{\gamma_1}{\gamma_0} - 1 \quad .$$

Another constraint for optimization was that e_b may never exceed an error threshold of 25%, even if this would result in a higher cumulative error. This constraint kept the effective spring rate C^* of a cluster from being significantly lower than the c_2 values assigned to this cluster by the optimization algorithm.

Whenever n clusters are described by n effective spring rates C^*, the sample space has the following form

$$\Omega = \left\{\left(C_{i_1}^*, \dots, C_{i_n}^*\right) \mid \; i_1, \dots, i_n \in \{1, \dots, N\} \text{ with } \; i_l \neq i_m \; \text{ for } \; l \neq m \right\} \quad .$$

Table 5 presents the results for different numbers of clusters, with E being the cumulative squared error for the given tuple $\Gamma = \left(\check{C}_{i_1}^*, \dots, \check{C}_{i_n}^*\right)$ (see above) that aggregates the effective cluster values that most accurately correlate with the c_2 values of all body locations. The values for E indicate that the more clusters there are, the more accurate the overall result becomes. While not surprising, this makes determining a minimum number of clusters difficult. Table 5 presents all results without of prioritizing any one.

Table 4. The optimization algorithm's results for differently sized clusters

n	E	C_1 [N/mm]	C_2 [N/mm]	C_3 [N/mm]	C_4 [N/mm]	C_5 [N/mm]
2	3.00	25	150	-	-	-
3	2.78	25	40	150	-	-
4	2.64	10	25	40	150	-
5	2.60	10	25	40	75	150

Table 5. Cluster values assigned to body locations for different cluster sizes $n = \{2, \dots, 5\}$

Body part	Body location	$C_{n=2}$ [N/mm]	$C_{n=3}$ [N/mm]	$C_{n=4}$ [N/mm]	$C_{n=5}$ [N/mm]
Head and neck	(1) Forehead	150	150	150	150
	(2) Temple	150	40	40	40
	(3) Masticatory muscle	25	25	25	25
	(4) Neck muscle	25	25	25	25
	(5) 7th cervical vertebra	25	25	25	25
Trunk	(6) Shoulder joint	25	25	25	25
	(7) 5th lumbar vertebra	150	40	40	75
	(8) Sternum	25	40	40	40
	(9) Pectoral muscle	25	25	10	10
	(10) Abdominal muscle	25	25	10	10
	(11) Pelvic bone	150	150	150	150
Upper extremities	(12) Deltoid muscle	25	25	10	10
	(13) Humerus	25	25	25	25
	(14) Radial bone	150	40	40	40
	(15) Forearm muscle	25	25	25	25
	(16) Arm nerve	25	25	25	25
Hand and fingers	(17)/(18) Forefinger pad	150	150	150	150
	(19)/(20) Forefinger end joint	150	150	150	150
	(21) Thenar eminence	150	40	40	40
	(22)/(23) Palm	150	150	150	75
	(24)/(25) Back of the hand	150	150	150	75
Lower extremities	(26) Thigh muscle	25	25	25	25
	(27) Kneecap	150	150	150	150
	(28) Middle of shin	150	150	150	150
	(29) Calf muscle	25	25	25	25

4 Discussion

The techniques and data used throughout this study can affect the quality of the corridors developed in a variety of ways. The following analyzes the techniques' impact on the corridors and examines constraints that affect the overall accuracy of the stiffness parameters.

4.1 Processed Data

Our data came from impact tests we performed with human subjects from 2015 to 2019. Since we decided against performing impact tests on the (4) neck muscle because of the serious health risks, we had to analyze the data from Melia et al. (2019) to estimate the desired stiffness parameters for (4) neck muscle. Their data from tests on (3) masticatory m. and (4) neck m. are distributed similarly. Only the mean values differ slightly. The mean value for (4) in particular is 1.2 times greater than the mean value of (3). Based on this finding, we presume that the stiffness parameters and the transition point for (3) and (4) differ from each other similarly.

Only data from impact tests with the F-Q10 contact body (see Figure 5) were processed in the study. The corridors and parameters determined are consequently only valid for loads applied by this contact body. Should the study results be used later to verify a PFMD's response, a contact body must be employed, which is identical to F-Q10 in terms of shape, material, and dimensions.

4.2 Modification of the Development Technique

As explained in section 2.2, none of the development techniques surveyed except for the one put forth by Lessley et al. (2002) had similarities with the technique we employed in a previous human subject study to calculate biomechanical limit values. Instead of normalized-deformation signals, we processed normalized-force signals with the technique devised by Lessley et al. to extract time increments for a list of equidistant and ascending normalized force values. Then, we used the time increments to determine the associated force and deformation value from the original signals. Normalizing the force signals ensured that the time increments extracted for $p = 1$ (100% being the maximum value of all normalized force signals) correspond to the maximum force values of the original force signals (not normalized) from which the limits were calculated in the other study.

The deformation and force values sampled for a specific percentage value were used to estimate the parameters of a log-normal cumulative distribution function (CDF). We then calculated the 25th, 50th, and 75th percentiles of the deformation and force values from the inverted CDF. Afterward, the percentiles were transferred to the deformation-force plane to plot the corridor curves and the candidate curve. To the best of our knowledge, a statistical model has never been incorporated in a biomechanical corridor development technique. Instead of percentiles, most techniques use the mean and standard deviation of the sampled deformation and force values. The CDF makes it very easy to relate the desired candidate curve to any percentiles. The data must meet two specific conditions, though. First, the number of sampled deformation and force values must be sufficient to estimate distribution parameters. Second, the sampled values must conform to the expected distribution (log-normal distribution here). The values we sampled in this study for normalized forces in the range of 10% to 100% met both conditions. An Anderson-Darling test was performed to confirm that the values conform to a log-normal distribution.

The confidence intervals of the percentiles were not considered in this study. We expect the confidence interval of the 50th percentile, e.g., to produce boundary curves that differ from the boundaries developed from the 25th and 75th percentile. The confidence intervals of the percentiles that describe the candidate curve could be a useful measure for specifying the acceptable deviation of a PFMD's deformation-force response.

4.3 Approximation of the Corridor Curves and Clustering

While the stiffness parameters and transition points derived from the piecewise-linear approximation of the candidate curves must be treated as a simplified representation of the nonlinear candidate curves, their values nevertheless specify the requisite features of future pressure-force measurement devices. Manufacturers must, therefore, ensure that their devices accurately replicate the response to pinching loads from F-Q10 (see section 4.1). A PFMD configuration for a specific body location is only acceptable when its deformation-force curve matches the associated approximation lines (see Appendix A) or lies above them. Otherwise, it will not replicate human biomechanics with sufficient accuracy and might deliver optimistic results.

The values for c_2 are not evenly distributed in the solution space spanned by the rates of commercially available springs. Body locations with low and high c_2 values are in fact more dominant than

those with values in between. The total error used for optimization consequently does not reflect this unequal distribution. Factoring in the distribution would have required to weighting the individual relative errors before aggregating them. The appropriate weighting technique is an open question, though. Since we decided to aggregate all individual errors without weighting in this study, the total error for $n = 4$ and $n = 5$ only differs by 1.5%. Even though the difference is small, we recommend using all available springs ($n = 5$) to obtain an optimal compromise between safety and efficiency.

4.4 Pressure Measurement

Pressure measurement is essential to the assessment of risk of injury posed by human-robot collisions, especially if the contact areas are small and tend to create regions of high normal stress (peak pressures). Currently available pressure sensors typically use thin sensitive films to measure the distribution of force within contact areas. Such films must be kept from wrinkling or creasing in order to prevent them from measuring peak pressures that are unrealistically higher than what contact would actually generate. Accurate replication of the approximated or original candidate curve, however, would require applying a compliant soft layer to the PFMD's impactor plate. Unfortunately, the soft layers required for precise replication are so compliant that they cannot prevent pressure films from wrinkling. Only SH70 materials (see section 3.3) allow both compliance and accurate pressure measurement. Such materials are in fact far too stiff to reproduce the toe of any corridor curve. Since the pressure on more compliant soft layers cannot be measured, the parameter c_1 and the transition point (d_T, F_T) can be disregarded as future PFMD design parameters.

Disregarding the candidate curves' toe lowers the amount of energy a PFMD can absorb in collision tests. The more energy a PFMD can absorb, the higher a robot's biomechanically safe speed can be. Although the loss of absorbable energy is small, disregarding the curves' toe entails another simplification of human biomechanics that diminishes cobots' overall efficiency. We, therefore, recommend exploring alternative pressure measurement technologies that can tolerate large deformations. Larger deformations would ultimately enable PFMDs to absorb more energy and thus robot users to operate their cobots faster without compromising safety.

4.5 Scaling and Effective Cluster Values

Before we could assign the parameter values from the approximation to cluster values, we had to determine the overall (or effective) stiffness of the soft layer and the spring. The two compliant elements can be treated as two springs arranged in a series. Since a PFMD must be able to measure pressure, the soft layer's material has to have a minimum shore A hardness of 70 (SH70). The effective stiffness C^* was calculated for a SH70 material loaded by F-Q10 and combined with a selection of commercially available springs. The overall stiffness would in fact be different if a different contact body had loaded the SH70 material since a soft material's effective stiffness is also affected by the contact area to which the load is applied. Since we scaled the parameter values obtained from the approximation (see section 2.4.2), whether F-Q10, which replicates semi-sharp contact, is the right contact body for determining C^* anyway is open to question.

Scaling the parameter values converted them into values that describe the biomechanical response to blunt contact. We used a compliant contact body (F-C30) in the human subject study to replicate blunt contacts. The data obtained from these tests cannot be used to develop corridors since the deformation signals recorded with F-C30 also include the deformation of the contact body, which we could neither measure nor compensate. We decided to use F-Q10 when determining the overall stiffness C^* because it replicates smaller contact areas common in industrial settings well. Since any contact area with dimensions larger than F-Q10 produces higher C^* values, the C^* values measured with F-Q10 can be considered conservative.

Another critical point is the selection of the springs and the conditions for assigning the c_2 values and their associated body locations to clusters. As mentioned, we only examined commercially available springs. Whenever the error e_b was not between -25% and 25%, the pertinent body location was assigned to a cluster associated with a spring rate significantly higher than the body location's c_2 value. For $n = 4$ clusters, there are five body locations with errors below -25%. Clusters' spring rates that exceed the c_2 values of the pertinent body locations by more than 25% are treated as conservative substitutes for the body locations. We have only three cases for $n = 5$ clusters. The error threshold and the commercially available springs used are the main reasons for the substantial difference in the PFMD's response from humans' natural response. It might be possible to compensate for the inaccuracies by adjusting the biomechanical limits for the different energies a PFMD and a human can absorb.

5 Conclusion

In this report, we presented a study with the objectives of (i) developing biomechanical response corridors from the data from human subject studies and (ii) deriving stiffness parameters from these corridors for future pressure-force measurement devices used to test cobots against biomechanical limits. We adopted the technique devised by Lessley et al. (2002) to develop the corridors since it enables us to incorporate the same statistical model we used in the human subject studies to calculate biomechanical limits. The corridors we developed include a candidate curve representing the 75th percentile of the force values and the 50th percentile of the deformation values measured in the human subject studies. The candidate curves were then approximated by two lines. The first line reproduces the candidate curve's toe and the second its linear section. Both lines are defined by slope parameters that equal stiffness parameters. Since the data processed come from tests with a semi-sharp contact body, they had to be converted to blunt contacts by scaling the parameter values. We decided to focus on the slope parameters of the second part of the linear approximations in order to simplify the desired stiffness parameters for future PFMDs. Then, we clustered these slope parameters, each cluster being defined by the effective stiffness of a SH70 material and spring in a series.

We discovered that accuracy improves as the number of different clusters increases. Although the best accuracy might seem desirable, we recommend using the results we obtained with $n = 5$ clusters corresponding to five springs with different rates.

We made several simplifications to ensure that a PFMD is easy to use and pressure measurements can be taken. Every simplification had a negative effect on the accuracy with which the final cluster values reproduce the humans' biomechanical response at the body locations analyzed. The loss of accuracy directly translates into a reduction of the efficiency of cobots validated by measurements with a PFMD. Different technical limitations preclude creating a PFMD that responds to robot impacts exactly as humans do. A PFMD with a soft layer and a spring that replicate human biomechanics will always be an inaccurate surrogate for humans. One way to reduce efficiency losses is to adjust the limits to allow a PFMD to absorb as much energy as the corridor's candidate curves.

A Biomechanical Corridors for All Body Locations

The following graphs present the biomechanical response corridors, candidate curves, and piece-wise-line approximation of the candidate curves for all body locations tested in the Fraunhofer IFF's human subject studies.

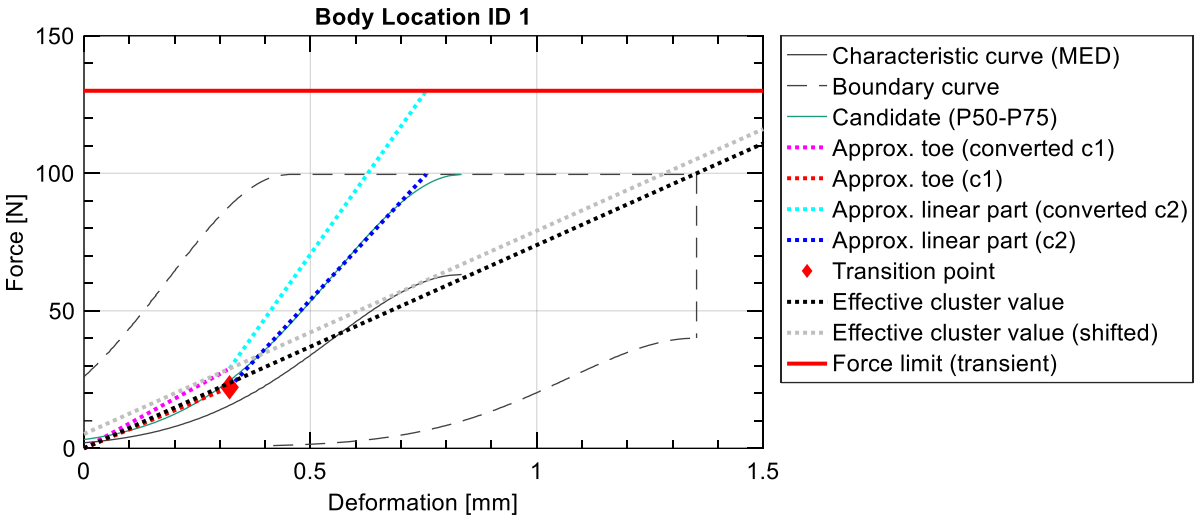

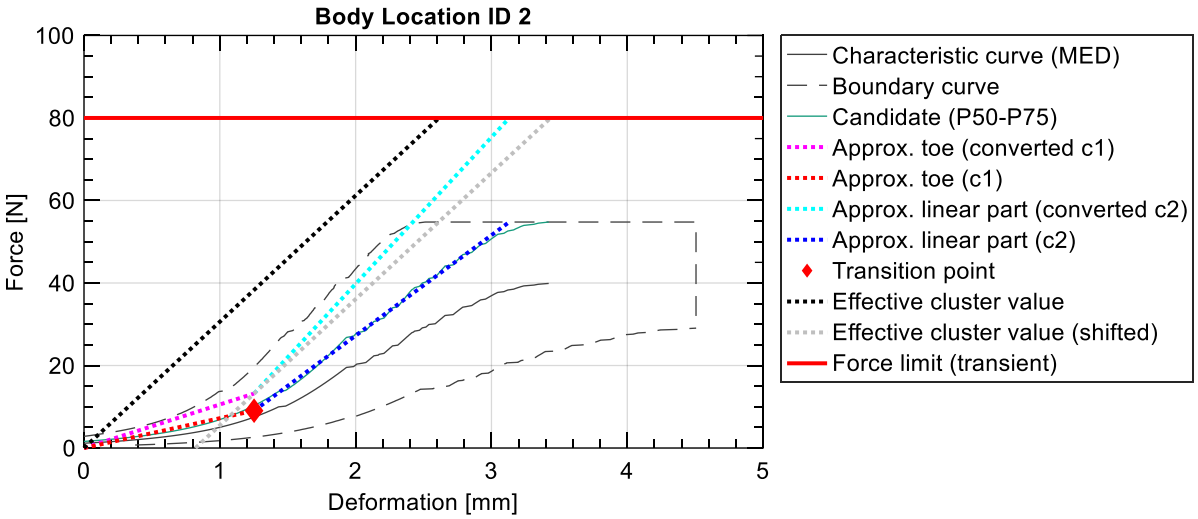

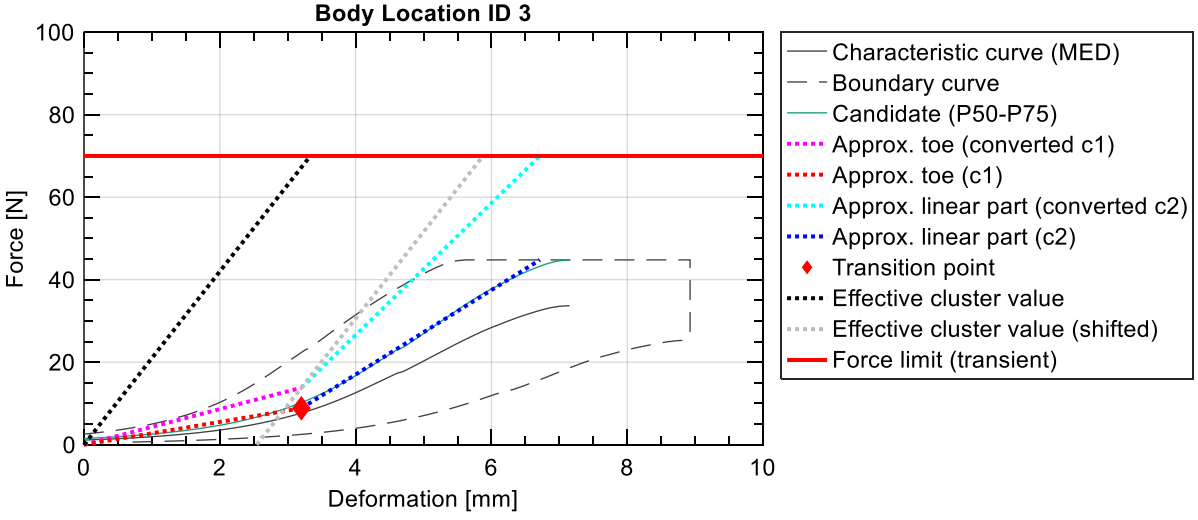

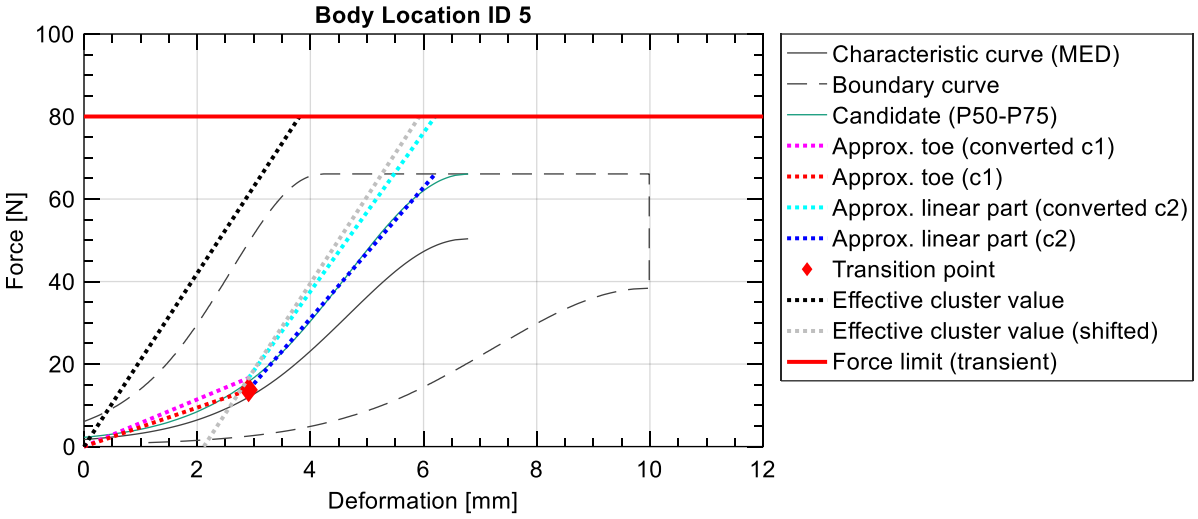
Body Location ID 5
Force [N]
Deformation [mm]
Characteristic curve (MED)
Boundary curve
Candidate (P50-P75)
Approx. toe (converted c1)
Approx. toe (c1)
Approx. linear part (converted c2)
Approx. linear part (c2)
Transition point
Effective cluster value
Effective cluster value (shifted)
Force limit (transient)

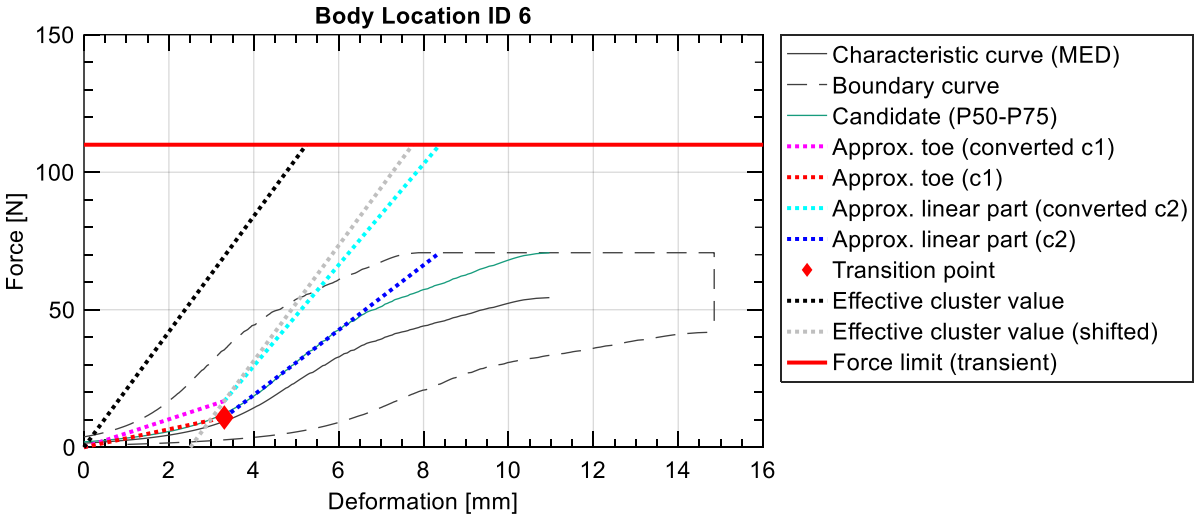
Body Location ID 6
Force [N]
Deformation [mm]
Characteristic curve (MED)
Boundary curve
Candidate (P50-P75)
Approx. toe (converted c1)
Approx. toe (c1)
Approx. linear part (converted c2)
Approx. linear part (c2)
Transition point
Effective cluster value
Effective cluster value (shifted)
Force limit (transient)

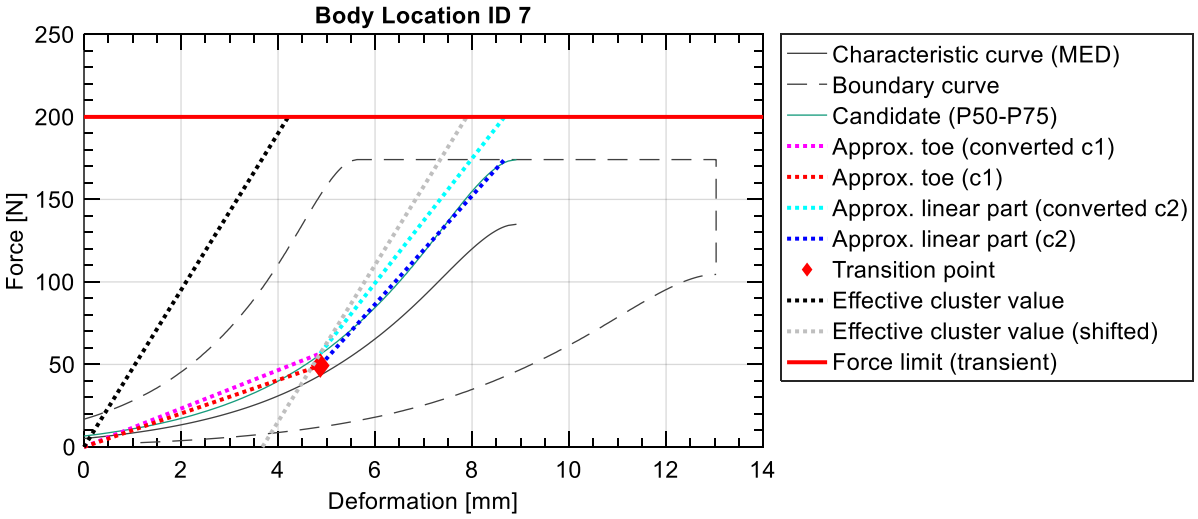
Body Location ID 7
Force [N]
Deformation [mm]
Characteristic curve (MED)
Boundary curve
Candidate (P50-P75)
Approx. toe (converted c1)
Approx. toe (c1)
Approx. linear part (converted c2)
Approx. linear part (c2)
Transition point
Effective cluster value
Effective cluster value (shifted)
Force limit (transient)

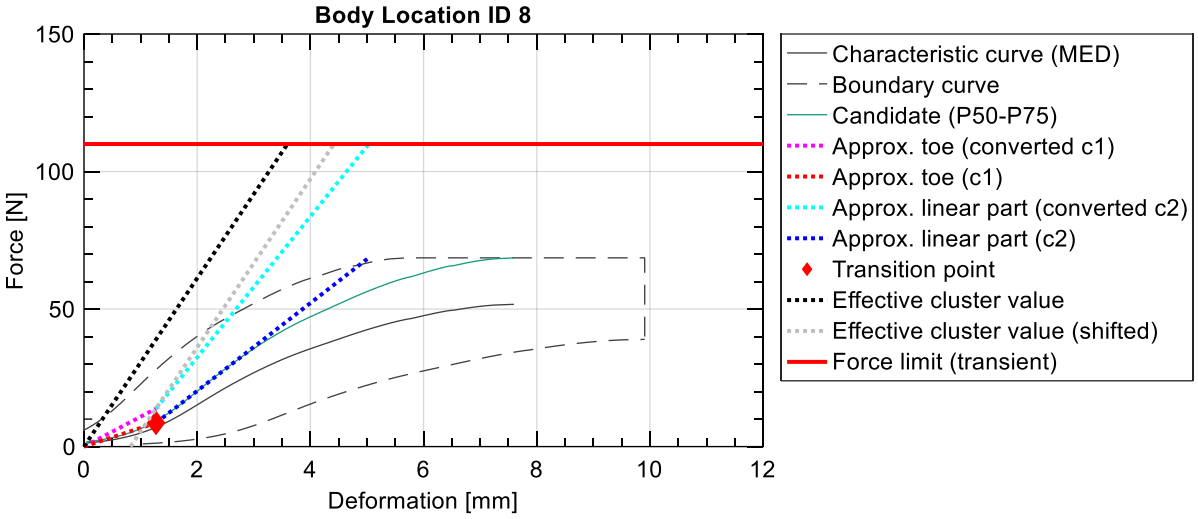
Body Location ID 8
Force [N]
Deformation [mm]
Characteristic curve (MED)
Boundary curve
Candidate (P50-P75)
Approx. toe (converted c1)
Approx. toe (c1)
Approx. linear part (converted c2)
Approx. linear part (c2)
Transition point
Effective cluster value
Effective cluster value (shifted)
Force limit (transient)

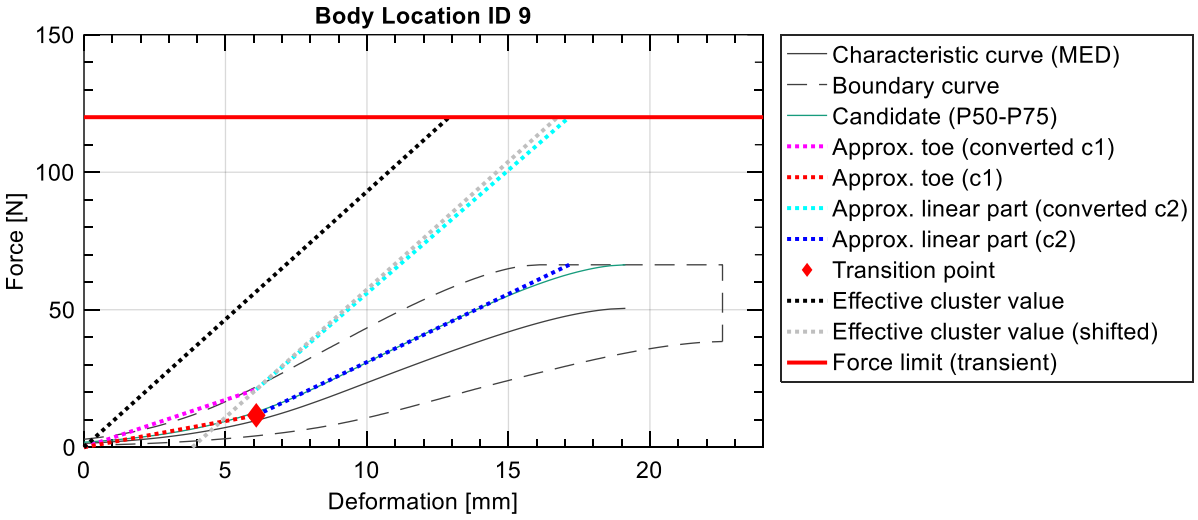
Body Location ID 9
Force [N]
Deformation [mm]
Characteristic curve (MED)
Boundary curve
Candidate (P50-P75)
Approx. toe (converted c1)
Approx. toe (c1)
Approx. linear part (converted c2)
Approx. linear part (c2)
Transition point
Effective cluster value
Effective cluster value (shifted)
Force limit (transient)

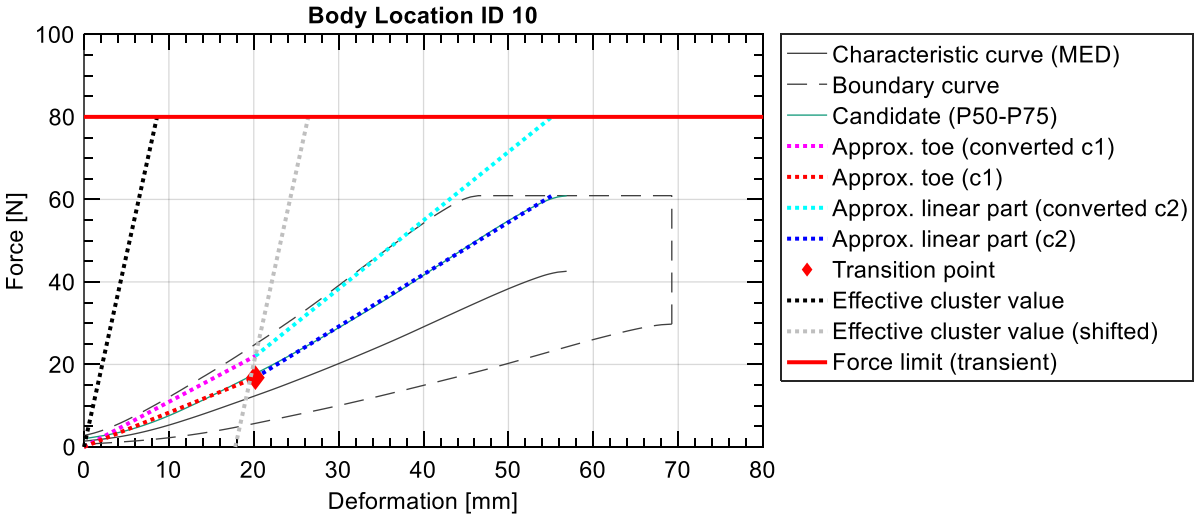
Body Location ID 10
Force [N]
Deformation [mm]
Characteristic curve (MED)
Boundary curve
Candidate (P50-P75)
Approx. toe (converted c1)
Approx. toe (c1)
Approx. linear part (converted c2)
Approx. linear part (c2)
Transition point
Effective cluster value
Effective cluster value (shifted)
Force limit (transient)

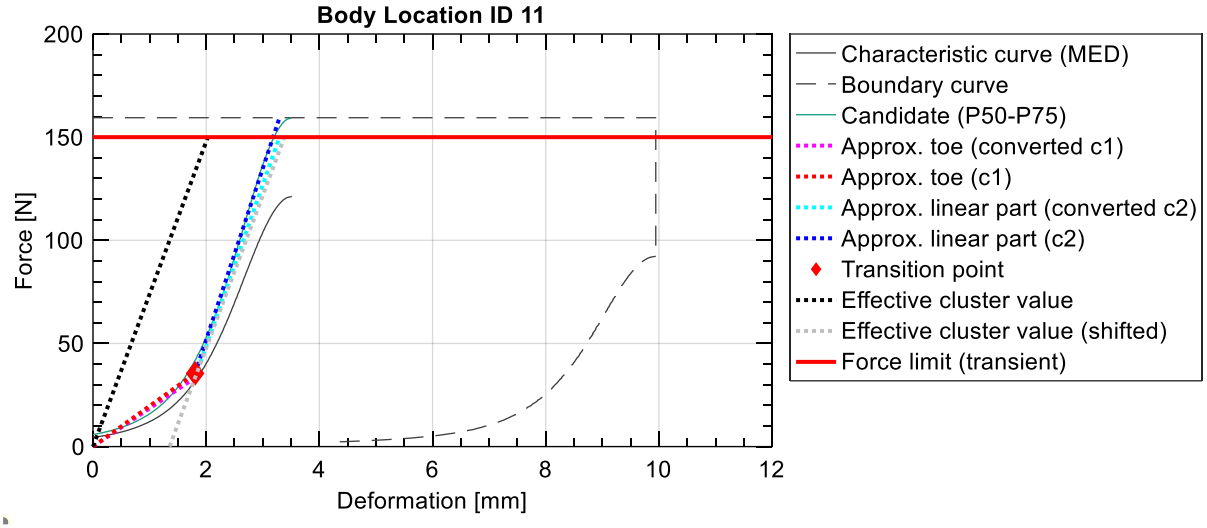
Body Location ID 11
Force [N]
Deformation [mm]
Characteristic curve (MED)
Boundary curve
Candidate (P50-P75)
Approx. toe (converted c1)
Approx. toe (c1)
Approx. linear part (converted c2)
Approx. linear part (c2)
Transition point
Effective cluster value
Effective cluster value (shifted)
Force limit (transient)

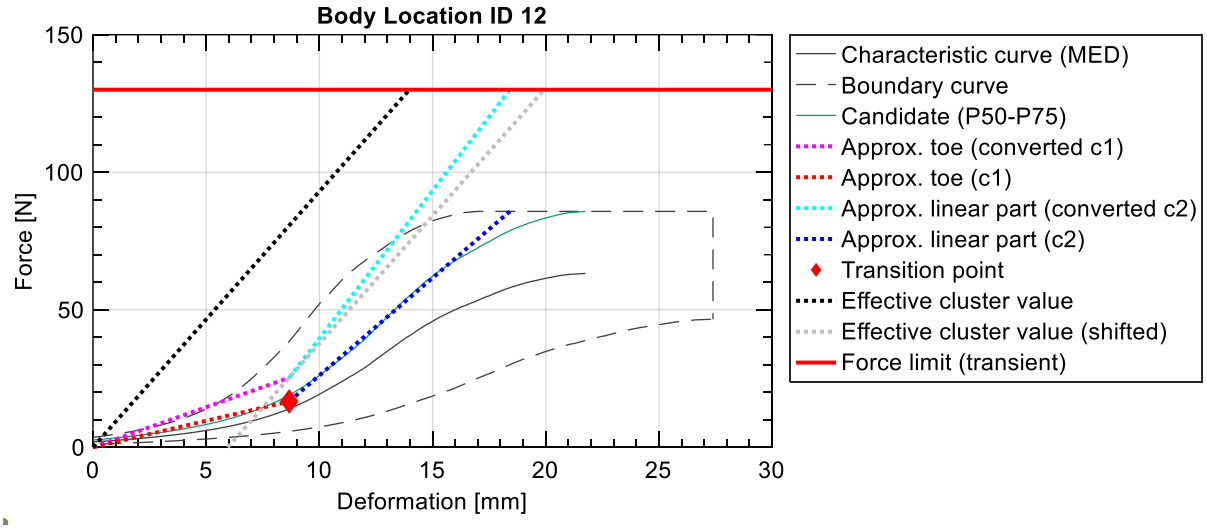
Body Location ID 12
Force [N]
Deformation [mm]
Characteristic curve (MED)
Boundary curve
Candidate (P50-P75)
Approx. toe (converted c1)
Approx. toe (c1)
Approx. linear part (converted c2)
Approx. linear part (c2)
Transition point
Effective cluster value
Effective cluster value (shifted)
Force limit (transient)

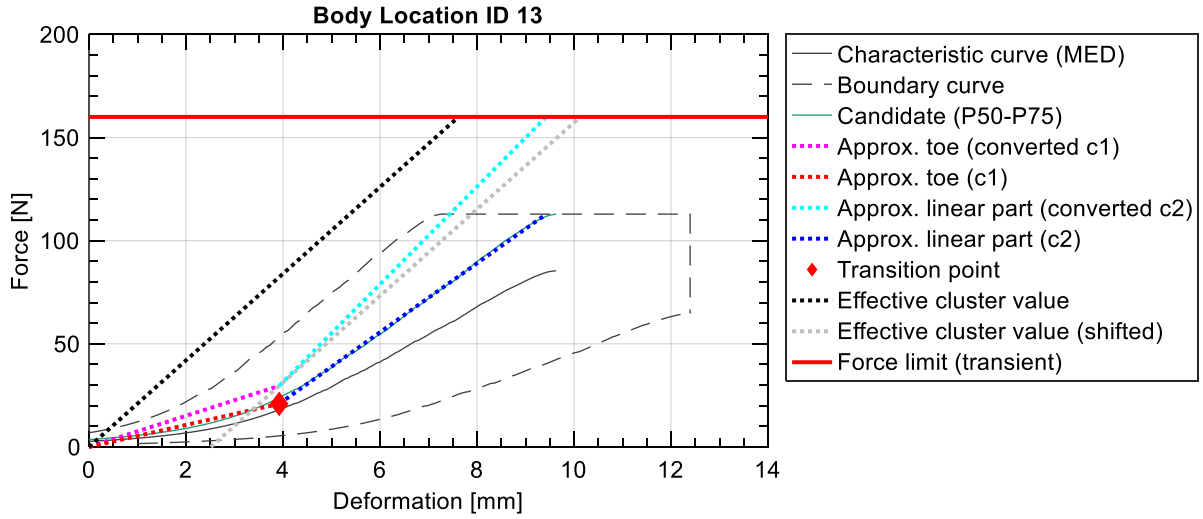
Body Location ID 13
Force [N]
Deformation [mm]
Characteristic curve (MED)
Boundary curve
Candidate (P50-P75)
Approx. toe (converted c1)
Approx. toe (c1)
Approx. linear part (converted c2)
Approx. linear part (c2)
Transition point
Effective cluster value
Effective cluster value (shifted)
Force limit (transient)

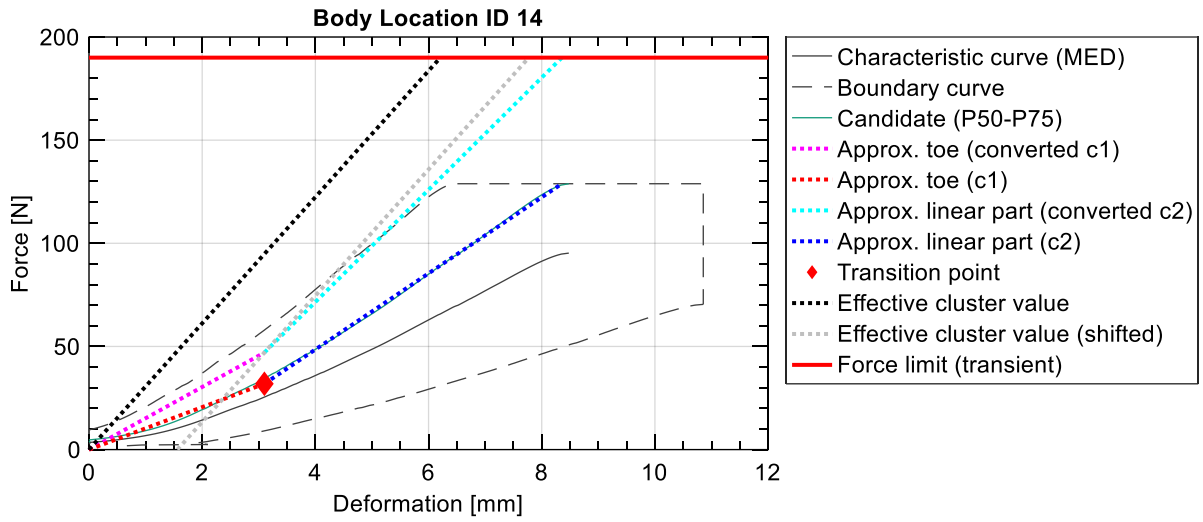
Body Location ID 14
Force [N]
Deformation [mm]
Characteristic curve (MED)
Boundary curve
Candidate (P50-P75)
Approx. toe (converted c1)
Approx. toe (c1)
Approx. linear part (converted c2)
Approx. linear part (c2)
Transition point
Effective cluster value
Effective cluster value (shifted)
Force limit (transient)

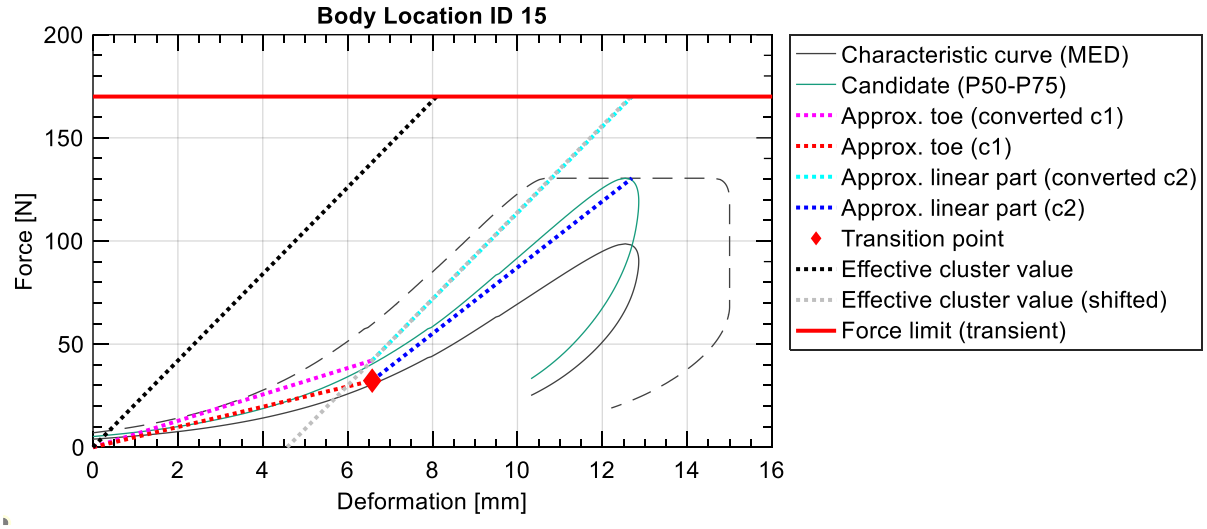
Body Location ID 15
Force [N]
Deformation [mm]
Characteristic curve (MED)
Candidate (P50-P75)
Approx. toe (converted c1)
Approx. toe (c1)
Approx. linear part (converted c2)
Approx. linear part (c2)
Transition point
Effective cluster value
Effective cluster value (shifted)
Force limit (transient)

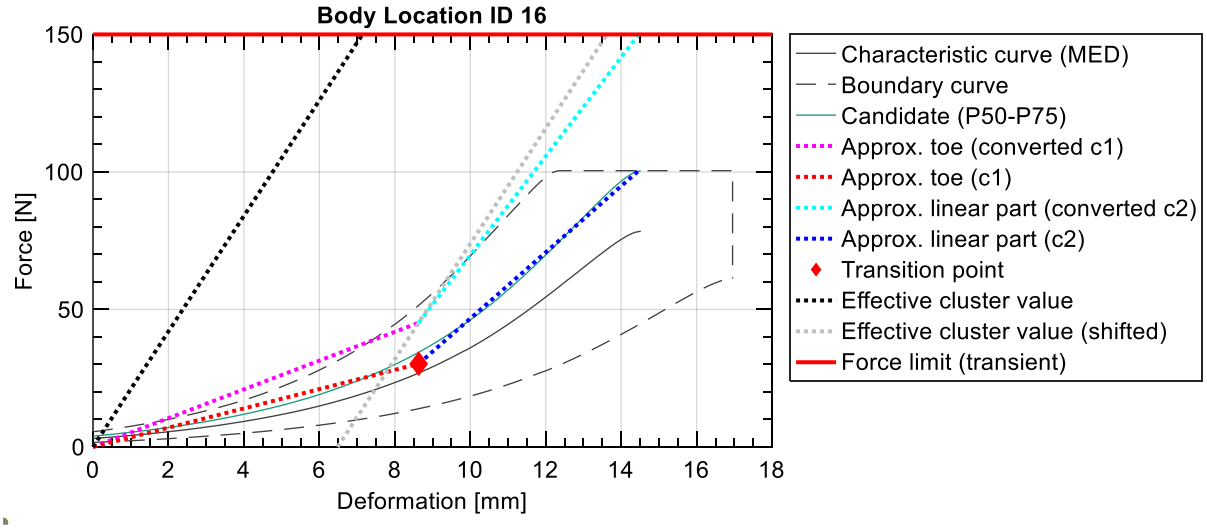
Body Location ID 16
Force [N]
Deformation [mm]
Characteristic curve (MED)
Boundary curve
Candidate (P50-P75)
Approx. toe (converted c1)
Approx. toe (c1)
Approx. linear part (converted c2)
Approx. linear part (c2)
Transition point
Effective cluster value
Effective cluster value (shifted)
Force limit (transient)

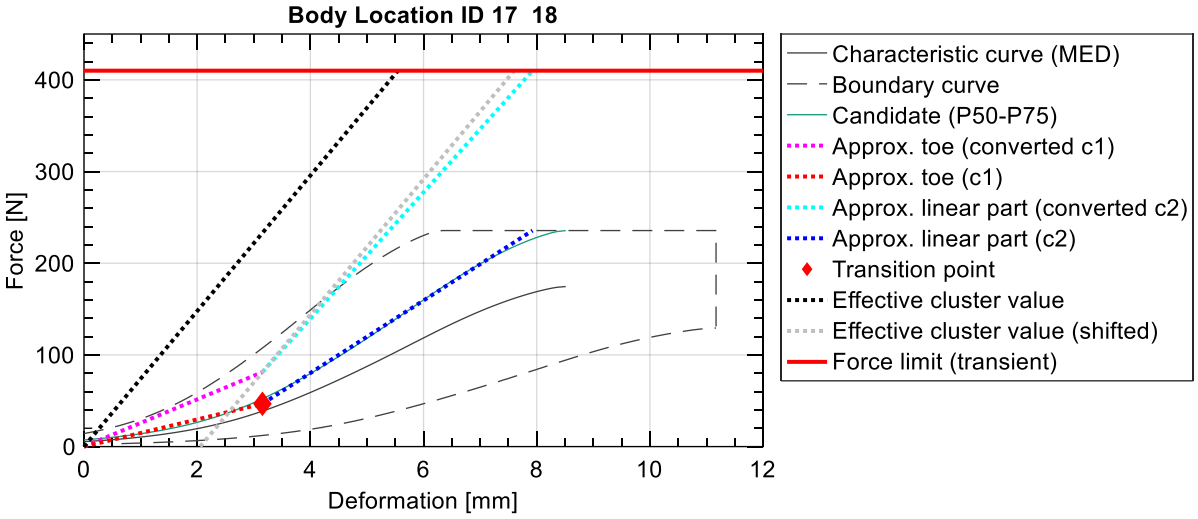
Body Location ID 17 18
Force [N]
Deformation [mm]
Characteristic curve (MED)
Boundary curve
Candidate (P50-P75)
Approx. toe (converted c1)
Approx. toe (c1)
Approx. linear part (converted c2)
Approx. linear part (c2)
Transition point
Effective cluster value
Effective cluster value (shifted)
Force limit (transient)

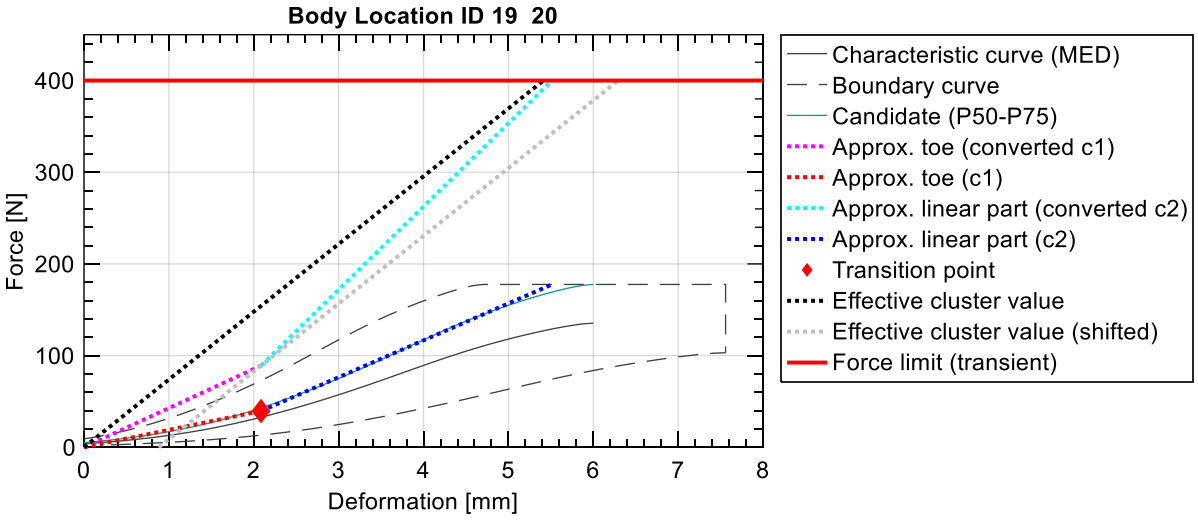
Body Location ID 19 20
Force [N]
Deformation [mm]
Characteristic curve (MED)
Boundary curve
Candidate (P50-P75)
Approx. toe (converted c1)
Approx. toe (c1)
Approx. linear part (converted c2)
Approx. linear part (c2)
Transition point
Effective cluster value
Effective cluster value (shifted)
Force limit (transient)

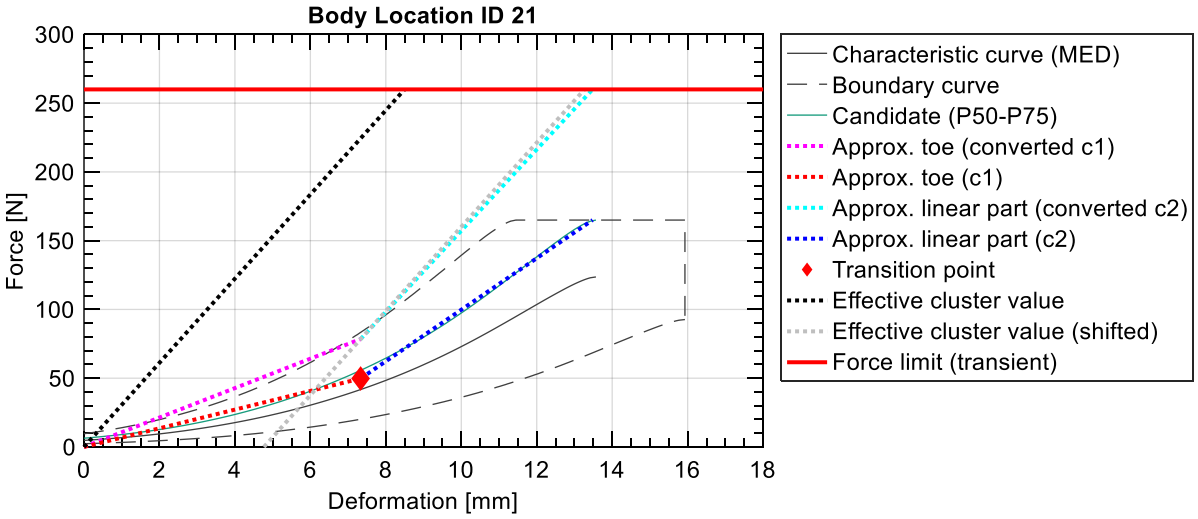
Body Location ID 21
Force [N]
Deformation [mm]
Characteristic curve (MED)
Boundary curve
Candidate (P50-P75)
Approx. toe (converted c1)
Approx. toe (c1)
Approx. linear part (converted c2)
Approx. linear part (c2)
Transition point
Effective cluster value
Effective cluster value (shifted)
Force limit (transient)

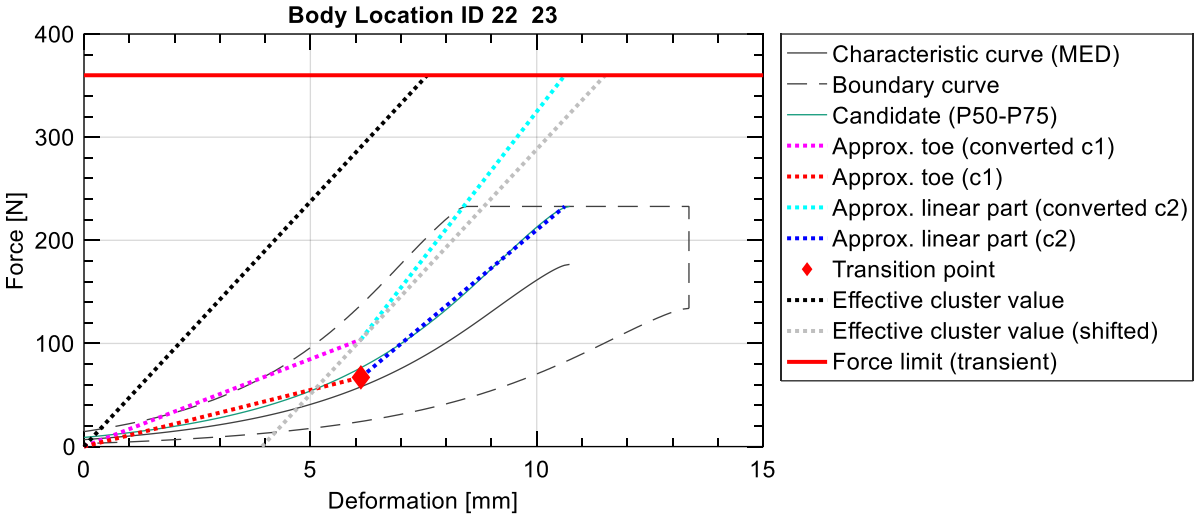
Body Location ID 22 23
Force [N]
Deformation [mm]
Characteristic curve (MED)
Boundary curve
Candidate (P50-P75)
Approx. toe (converted c1)
Approx. toe (c1)
Approx. linear part (converted c2)
Approx. linear part (c2)
Transition point
Effective cluster value
Effective cluster value (shifted)
Force limit (transient)

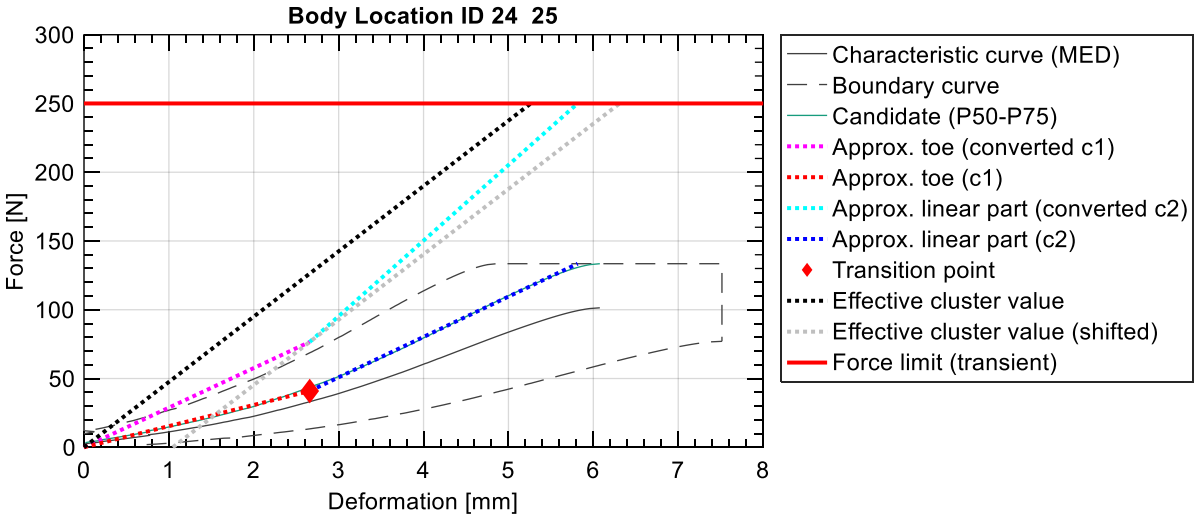
Body Location ID 24 25
Force [N]
Deformation [mm]
Characteristic curve (MED)
Boundary curve
Candidate (P50-P75)
Approx. toe (converted c1)
Approx. toe (c1)
Approx. linear part (converted c2)
Approx. linear part (c2)
Transition point
Effective cluster value
Effective cluster value (shifted)
Force limit (transient)

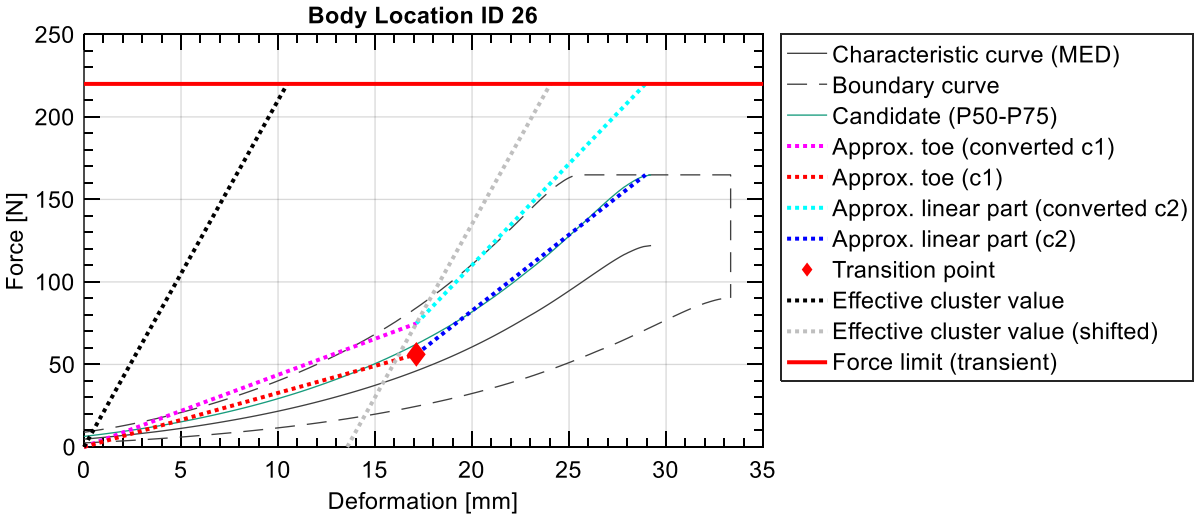
Body Location ID 26
Force [N]
Deformation [mm]
Characteristic curve (MED)
Boundary curve
Candidate (P50-P75)
Approx. toe (converted c1)
Approx. toe (c1)
Approx. linear part (converted c2)
Approx. linear part (c2)
Transition point
Effective cluster value
Effective cluster value (shifted)
Force limit (transient)

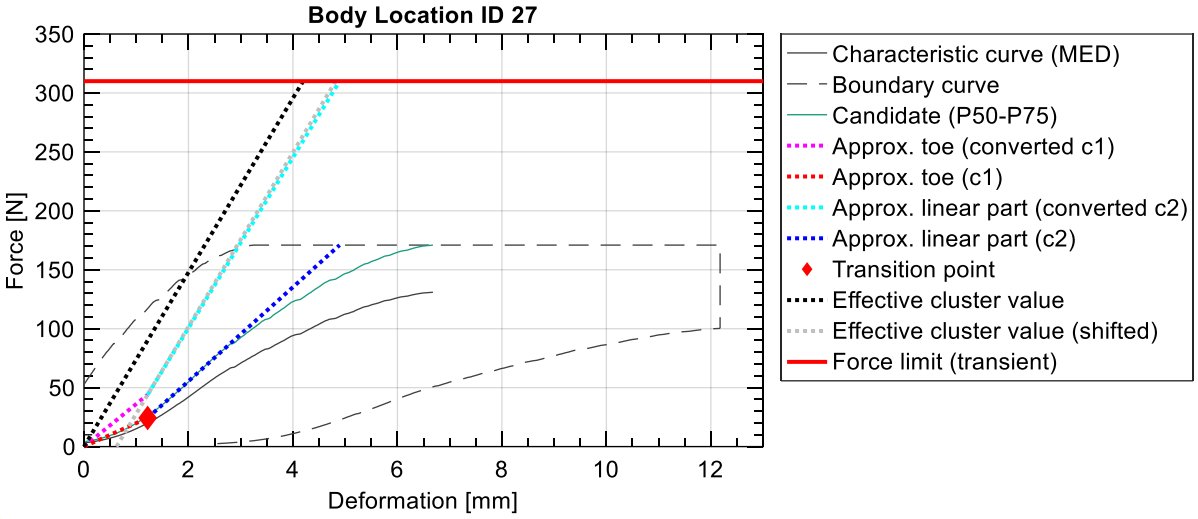
Body Location ID 27
Force [N]
Deformation [mm]
Characteristic curve (MED)
Boundary curve
Candidate (P50-P75)
Approx. toe (converted c1)
Approx. toe (c1)
Approx. linear part (converted c2)
Approx. linear part (c2)
Transition point
Effective cluster value
Effective cluster value (shifted)
Force limit (transient)

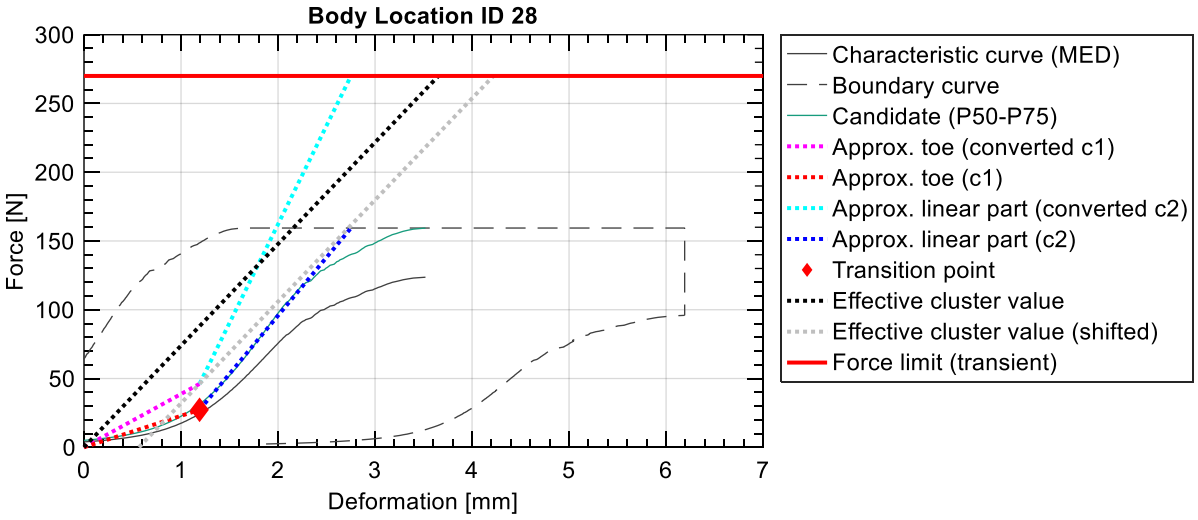
Body Location ID 28
Force [N]
Deformation [mm]
Characteristic curve (MED)
Boundary curve
Candidate (P50-P75)
Approx. toe (converted c1)
Approx. toe (c1)
Approx. linear part (converted c2)
Approx. linear part (c2)
Transition point
Effective cluster value
Effective cluster value (shifted)
Force limit (transient)

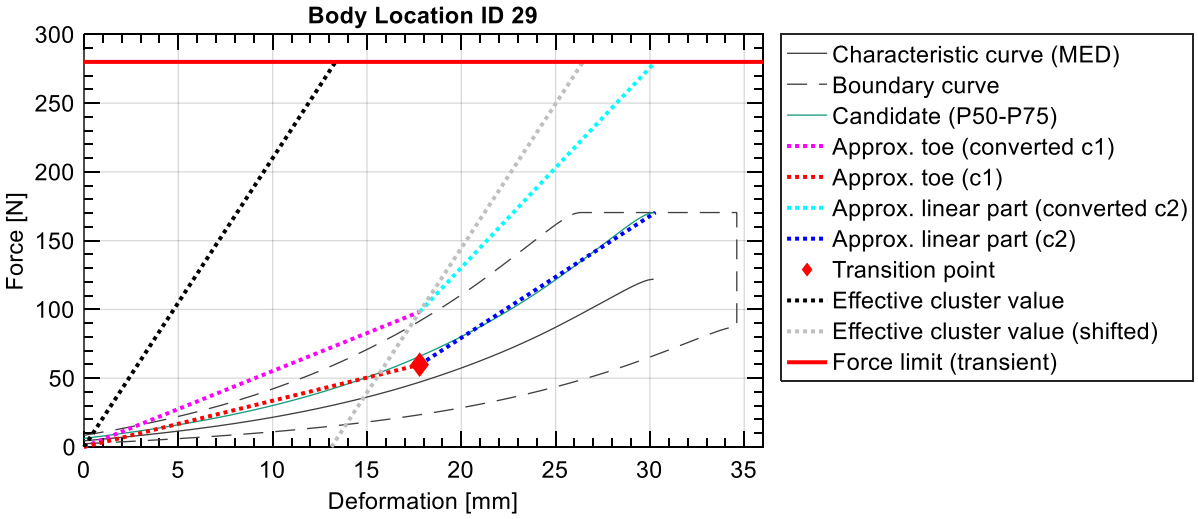
Body Location ID 29
Force [N]
Deformation [mm]
Characteristic curve (MED)
Boundary curve
Candidate (P50-P75)
Approx. toe (converted c1)
Approx. toe (c1)
Approx. linear part (converted c2)
Approx. linear part (c2)
Transition point
Effective cluster value
Effective cluster value (shifted)
Force limit (transient)

6 References

Bolte, John H.; Hines, Margaret H.; Herriott, Rodney G.; McFadden, Joseph D.; Donnelly, Bruce R. (2003): Shoulder Impact Response and Injury Due to Lateral and Oblique Loading. In: SAE Technical Paper Series. 47th Stapp Car Crash Conference (2003), OCT. 27, 2003: SAE International400 Commonwealth Drive, Warrendale, PA, United States (SAE Technical Paper Series).

Cavanaugh, J. M.; Nyquist, G. W.; Goldberg, S. J.; King, A. I. (1986): Lower Abdominal Tolerance and Response. Paper 861878. In: SAE Technical Paper Series: SAE International.

Eppinger, Rolf H.; Marcus, Jeffrey H.; Morgan, Richard M. (1984): Development of Dummy and Injury index for NHTSA's Thoracic Side Impact Protection Research Program. Paper 840885. In: SAE Technical Paper Series: SAE International.

Hsu, Timothy P.; Nusholtz, Guy S. (2005): Considerations of Bio-fidelity Corridors for Lateral Impacts. In: SAE Technical Paper Series. SAE 2005 World Congress & Exhibition, APR. 11, 2005: SAE International400 Commonwealth Drive, Warrendale, PA, United States (SAE Technical Paper Series).

Kim, T.; Shin, J.; Ye, X.; Crandall, J.; Knospe, C.; Funk, J. (2013): Evaluation of methods for the development of representative responses and corridors from biomechanical data using mechanical models. In: *INTERNATIONAL JOURNAL OF CRASHWORTHINESS* 18 (6), S. 633–646. DOI: 10.1080/13588265.2013.830946.

Lessley, David; Crandall, Jeff; Shaw, Greg; Kent, Richard; Funk, James (2002): A Normalization Technique for Developing Corridors from Individual Subject Responses. In: Proceedings of the Thirty-First International Workshop on Human Subjects for Biomechanical Research. NHTSA.

Maltese, Matthew R.; Eppinger, Rolf H.; Rhule, Heather H.; Donnelly, Bruce R.; PINTAR, FRANK A.; Yoganandan, Narayan (2002): Response Corridors of Human Surrogates in Lateral Impacts. In: SAE Technical Paper Series. 46th Stapp Car Crash Conference (2002), NOV. 11, 2002: SAE International400 Commonwealth Drive, Warrendale, PA, United States (SAE Technical Paper Series).

Melia, Michael; Geissler, Britta; König, Jochem; Ottersbach, Hans Jürgen; Umbreit, Matthias; Letzel, Stefan; Muttray, Axel (2019): Pressure pain thresholds: Subject factors and the meaning of peak pressures. In: *European journal of pain (London, England)* 23 (1), S. 167–182. DOI: 10.1002/ejp.1298.

Morgan, Richard M.; Marcus, Jeffrey H.; Eppinger, Rolf H. (1986): Side Impact - The Biofidelity of NHTSA's Proposed ATD and Efficacy of TTI. Paper 861877. In: SAE Technical Paper Series. 30th Stapp Car Crash Conference (1986): SAE International (SAE Technical Paper Series), S. 27–40.

Nusholtz, G. S.; Hsu, T. P.; Shi, Y.; Kochekseraii, S. B.; Luna, M. A. G. (2009): Creating Representative Curves from Multiple Time Histories of Vehicle, ATD and Biomechanics Tests. In: Proceedings of the 21st ESV, Bd. 21. International TechnicalConference on the Enhanced Safety of Vehicles (ESV). Stuttgart (Germany). NHTSA, S. 1–9.

Pungrasmi, T.; Shimaoka, Y.; Okamoto, T.; Watanabe, R. (2019): Contact Area Effects on Superficial and Deep Pain Threshold for Service Robot Safety Design using a Pain-sensing System. Development of a Human-inspired Pain-sensing System. In: *Panasonic Technical Journal* 65 (1), S. 21–27.

Raymond, David; Crawford, Greg; van Ee, Chris; Bir, Cynthia (2009): Development of biomechanical response corridors of the head to blunt ballistic temporo-parietal impact. In: *J Biomech Eng* 131 (9), S. 94506. DOI: 10.1115/1.3194751.

Shaw, Joshua M.; Herriott, Rodney G.; McFadden, Joseph D.; Donnelly, Bruce R.; Bolte, John H. (2006): Oblique and lateral impact response of the PMHS thorax. In: *Stapp car crash journal* 50, S. 147–167. DOI: 10.4271/2006-22-0007.

Stemper, Brian D.; Yoganandan, Narayan; PINTAR, FRANK A. (2004): Response Corridors of the Human Head-Neck Complex in Rear Impact. In: *Annual proceedings. Association for the Advancement of Automotive Medicine* 48, S. 149–163.

Sun, W.; Jin, J. H.; Reed, M. P.; Gayzik, F. S.; Danelson, K. A.; Bass, C. R. et al. (2016): A method for developing biomechanical response corridors based on principal component analysis. In: *Journal of biomechanics* 49 (14), S. 3208–3215. DOI: 10.1016/j.jbiomech.2016.07.034.